

Characterization and Guideline Development
of the Heat Staking Process

Royston DeSouza
Steven Zhao
Zhan Zhai

A thesis submitted in partial fulfilment
of the requirements for the degree of

BACHELOR OF APPLIED SCIENCE

Supervisors: W. L. Cleghorn
J. K. Mills

Department of Mechanical and Industrial Engineering

ABSTRACT

Autoliv's manufacturing culture of continuous process improvement was the motivation behind this thesis project. Currently Autoliv does not have an optimized process guideline for their heat staking technology. The challenge was to capture the effect of various machine process parameters on the quality of the heat stake joint with limited machine availability for testing. Four machine parameters including: Heating Time, Punch Pressure, Punch Time and Airflow Rate were investigated utilizing an efficient design of experiments. A four-factor-two-level full factorial design of experiments captured the linear relationships between the machine parameters and the quality of the heat stake joint, which was defined as the tensile strength and visual quality. Of the four initial machine parameters investigated, only punch time was found to be irrelevant to the quality of the heat stake joint. A correlation was discovered between heat stake joints with well-surrounded flash coverage and consistently high tensile strength. The optimal setting of the process parameters which provided greatest overall quality of the heat stake joint was solved through the application of a numerical optimizer. The optimal process settings are: Heating Time, Punch Pressure, Airflow Rate and Punch Time set at 6 seconds, 70 psi, 70 SCFH and 6.5 seconds respectively. At optimal settings, the tensile strength of the joint increased by thirty-three percent compared to initial settings. This information allows Autoliv to consistently produce high quality heat stake joints while easily monitoring the process through visual inspection.

ACKNOWLEDGEMENTS

We would like to thank the following people for their generous help and support.

From the University of Toronto faculty and staff:

- Professor W. L. Cleghorn
- Professor J. K. Mills
- David Nacson
- Tomas Bernreiter

From Autoliv Electronics Canada:

- Patrina Lambert
- Samir Ruparelia
- Victor Chu
- Careen Lawson
- Ken Ku
- Anthony Quattrocchi

From Tri-M Machine Works:

- Pablo de Jesus
- Marcel de Jesus Jr.

From Extol Inc.:

- Rod Kitchen

TABLE OF CONTENTS

1	Introduction.....	1
1.1	Autoliv Profile	1
1.2	Heat Staking Background	1
1.3	Autoliv Heat Stake Quality Specifications	3
1.4	Heat Staking Equipment	5
1.5	Objective.....	6
1.6	Scope.....	7
2	Project Methodology.....	8
2.1	Parameter Selection	8
2.2	Establishing Boundary Conditions	9
2.3	Design of Experiments.....	10
2.3.1	Response Equation.....	11
2.3.2	Justification of Utilizing the Design of Experiments Method	13
2.3.3	Full Factorial Design of Experiments	13
2.3.4	Fractional Factorial Design of Experiments	14
2.3.5	Experimental Strategy Selection.....	15
2.3.6	Designed Experiments	17
2.4	Tensile Strength Testing	19
2.4.1	Sample Generation.....	19
2.4.2	Visual Data Acquisition.....	26
2.4.3	Tensile Testing Experiment	28
2.4.3.1	Extraction of Heat Stake Joints.....	28
2.4.3.2	Tensile Testing Experiment Method.....	31
2.4.3.3	Customized Hardware.....	32
2.4.3.4	Financial Breakdown: Costs Related to Experiments.....	36
3	Analysis of Results	39
3.1	Results Overview.....	39
3.2	Heat Stake Joint Strength Results.....	40
3.3	Heat Stake Visual Quality Results.....	42
3.4	Visual Quality Correlation to Strength	43
3.5	Heat Stake Joint Strength Analysis.....	45
3.6	Heat Stake Visual Quality Analysis.....	50
3.7	Optimization	55
3.7.1	Optimizing Joint Strength.....	55
3.7.2	Optimizing Visual Quality.....	55
3.8	Final Optimization of Heat Staking Process Parameters	56
3.8.1	Validating Optimal Strength Values.....	57
3.8.2	Validating Optimal Visual Quality Values	58
3.9	Potential Failure Modes of the Heat Staking Process.....	59
4	Conclusion and Recommendations.....	60
5	References.....	63

LIST OF FIGURES

- Figure 1-1 Pre-heat staked post and circuit board
- Figure 1-2 Heat staked post and circuit board
- Figure 1-3 Side view of heat staked post and circuit board
- Figure 1-4 Joint cross-section depicting complete seating of heat stake head
- Figure 1-5 Unacceptable punch imprint
- Figure 1-6 Schematic representation of the heat staking process
- Figure 2-1 P-Diagram of heat staking process
- Figure 2-2 Back pressure provided by circuit board required for head formation
- Figure 2-3 Malformed heat stake head resulting from inadequate back pressure
- Figure 2-4 Mother panel containing four bare daughter boards
- Figure 2-5 Mother panel undergoing routing process
- Figure 2-6 Heat staking machine within the assembly dial table
- Figure 2-7 Close-up of the heat staking nozzles
- Figure 2-8 Reference visual quality image
- Figure 2-9 Measurement of flash on heat stake head
- Figure 2-10 Heat stake base locations within the module
- Figure 2-11 Cutting planes used to extract the heat stakes
- Figure 2-12 Induced loads during cutting operation
- Figure 2-13 Heat stakes extracted from the module
- Figure 2-14 Preliminary tensile testing method: manual loading
- Figure 2-15 Clamping the heat stake sample without a fixture

Figure 2-16 Design of the tensile test fixture

Figure 2-17 Force loading on a heat stake sample for the selected fixture

Figure 2-18 Heat stake sample testing in Instron Machine

Figure 3-1 Visual quality values versus heat stake strengths

Figure 3-2 Pareto chart for heat stake joint strength analysis

Figure 3-3 Main effect plot for heat stake joint strength analysis

Figure 3-4 Interaction plot for heat stake joint strength analysis

Figure 3-5 Pareto chart for heat stake joint visual quality rating

Figure 3-6 Main effects plot for heat stake joint visual quality rating

Figure 3-7 Interaction plot for heat stake visual quality rating

LIST OF TABLES

- Table 1-1 Pass criteria of the heat stake joint
- Table 2-1 Boundary conditions of selected process parameters
- Table 2-2 Two level full factorial DOE with center point
- Table 2-3 L9 array DOE
- Table 2-4 Raw materials required to run trials
- Table 2-5 Visual quality metrics used in visual analysis
- Table 2-6 Financial breakdown for heat stake investigation
- Table 3-1 Tensile strength results for four-factor-two-level full factorial DOE with center point analysis
- Table 3-2 Tensile strength testing results of L9 array DOE
- Table 3-3 Visual quality results for four-factor-two-level full factorial DOE with center point analysis
- Table 3-4 Visual quality testing results of L9 array DOE
- Table 3-5 Mean and standard deviation strength for each visual quality rating
- Table 3-6 Summary of four-factor-two-level full factorial DOE with center point analysis
- Table 3-7 Heat stake joint visual rating analysis summary
- Table 3-8 Control factor setting for optimal strength response
- Table 3-9 Control factor setting for optimal visual quality response
- Table 3-10 Process parameter setting values after optimization
- Table 3-11 Potential failure modes associated with non-ideal settings

1 Introduction

1.1 Autoliv Profile

Autoliv Electronics Canada is an international automotive safety system manufacturer. Autoliv has developed safety electronics since 1987 including both airbag and seatbelt systems. The manufacturing plant in Markham Ontario specializes in assembling crash sensor modules, restraint and airbag control modules, as well as radar based cruise control central units. Autoliv has recently introduced heat staking technology to affix fibreglass circuit boards within plastic module housings, as an alternative to the costly process of fastening screws.

1.2 Heat Staking Background

Assembly is a major manufacturing process that typically involves joining components made from different materials. As a result, manufacturing companies have given much attention to effectively joining dissimilar materials. One solution is heat staking, which is a quick, economical and consistent process of joining plastics to other materials¹. A plastic post on one component is projected through a hole in the second component as shown in Figure 1-1. The post is plasticized by heating, and then pressed to form a dome over the hole of the second component, locking the two parts together, as shown in Figure 1-2 and Figure 1-3.

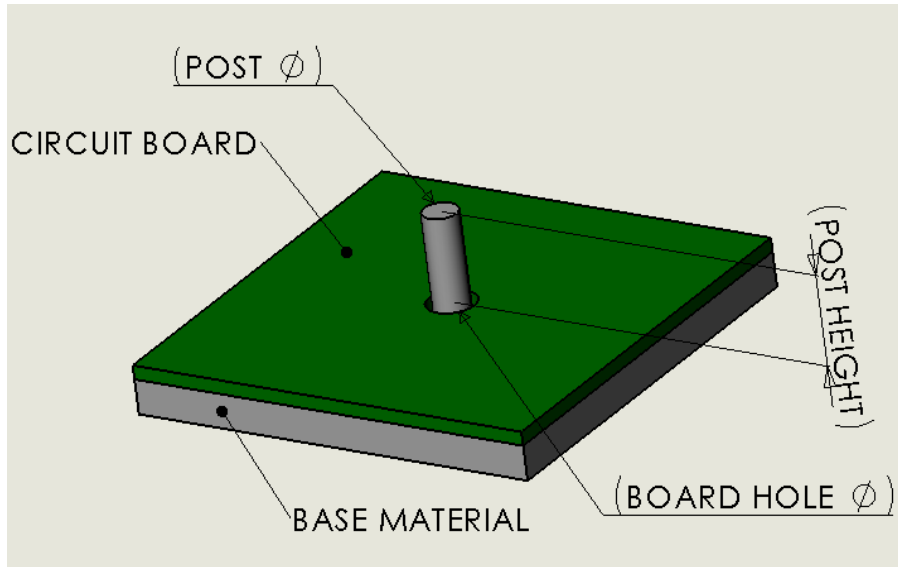


Figure 1-1 Pre-heat staked post and circuit board

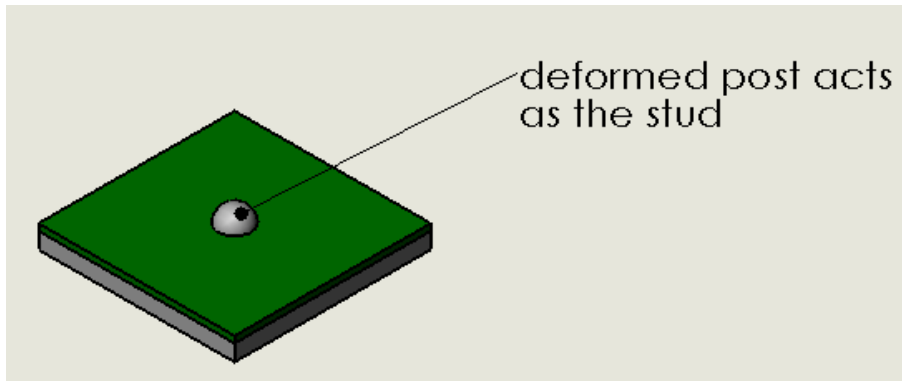


Figure 1-2 Heat staked post and circuit board

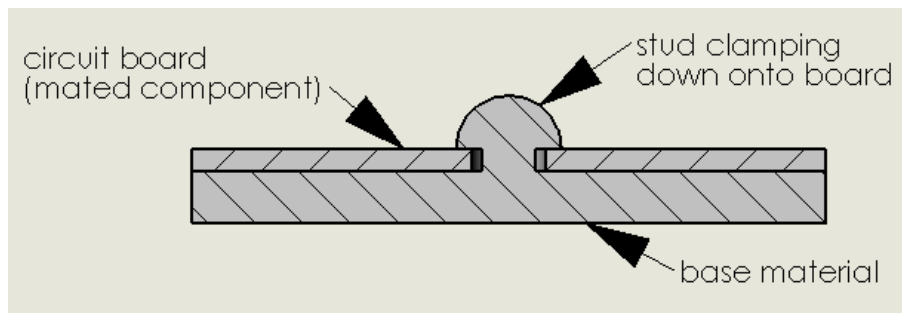


Figure 1-3 Side view of heat staked post and circuit board

The quality of a heat stake joint is characterized by its tensile strength, the amount of flash, and the completeness of the punch print on the heat stake dome. The quality of the joint is dependent on both the product parameters of the pre-heat skated plastic post and circuit board, as well as the process parameters of the heat staking equipment, as defined in Section 2.1.

1.3 Autoliv Heat Stake Quality Specifications

Through collaboration with Autoliv, several critical specifications were established as targets for the experimental samples. These specifications are the current standards that Autoliv adheres to in the current production setup and are termed “Pass Criteria”. It also includes a potential criterion regarding flash presence.

Primarily, an individual heat stake joint must sustain 267 Newtons (N) of axial tension. A second pass criterion requires that the heat stake head must be fully seated on the circuit board, meaning the distance between the bottom of the heat stake head and the circuit board is equal to 0 mm as shown in Figure 1-4.

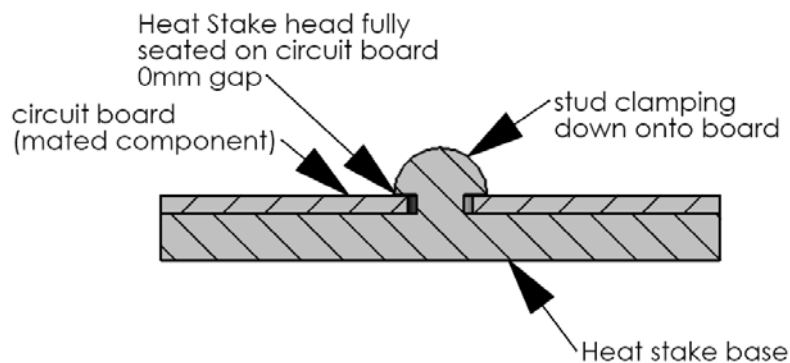


Figure 1-4 Joint cross-section depicting complete seating of heat stake head

A third pass criterion stipulates that after forming the heat stake joint, the punching form shape must be visible or imprinted around 100% of the circumference of the heat stake head. Figure 1-5 shows an unacceptable punch imprint due to an incomplete punch press.

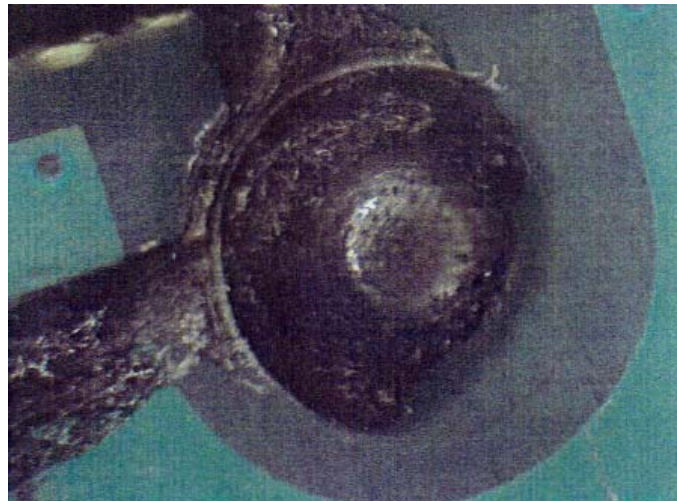


Figure 1-5 Unacceptable punch imprint

The established pass criteria were implemented during the sampling and testing stages of this thesis project to pass or fail the heat stake samples.

While there is no current pass criterion for the amount of flash present around a heat stake joint, Autoliv intends to develop a target specification that is based on a correlation between flash presence and joint strength. This specification will enable Autoliv to validate whether a heat stake passes the strength criterion by a visual inspection of the amount of flash present. Table 1-1 summarizes the four pass criteria.

Table 1-1 Pass criteria of the heat stake joint

Characteristic/Feature	Pass Criteria
Tensile Failure Strength	At least 267 N
Heat Stake Head (Dome) Height	Must be fully seated on circuit board
Punch (Form) Imprint	100% of circumference is visibly imprinted
Heat Stake Head Flash	To be developed from this project

1.4 Heat Staking Equipment

Autoliv utilizes InfraStake equipment manufactured by Extol to perform their heat stake operation. The heat staking process involves four phases: Heating & Clamping, Staking & Cooling, Punch & Head Retraction, and Cycle Completion. Figure 1-6 is a schematic representation of the heat staking process.

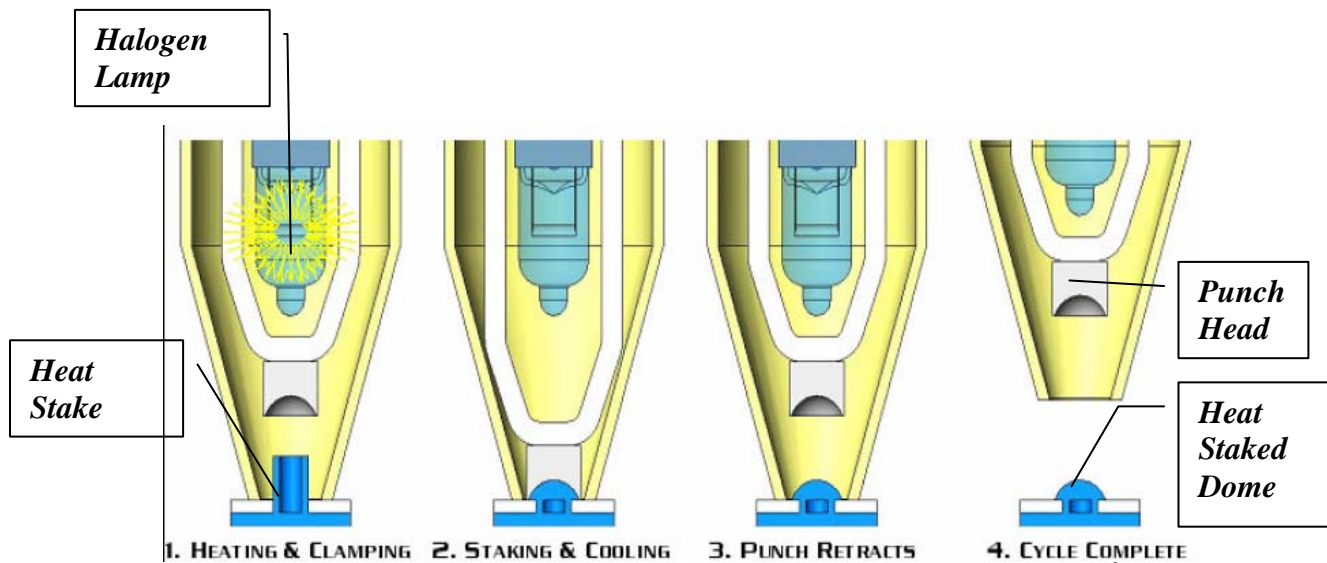


Figure 1-6 Schematic representation of the heat staking process²

Heating & Clamping:

The InfraStake punch head is positioned directly over the staking surface and initiates the heating cycle by illuminating the 100 Watt halogen grade lamp. The emitted infrared light is collimated and radially oriented so that it directly focuses on the plastic post for consistent heating.

Staking & Cooling:

At the end of the heating cycle the lamp is turned off and the low-impact air cylinder with integrated staking punch presses down and it forms over the semi-molten post.

Punch & Head Retraction:

The internal staking punch mechanism retracts at the end of the programmed hold time.

Cycle Completion:

The heat staking cycle is completed with the punch and head at their original position, and is ready for the next cycle.

1.5 Objective

The objective of the thesis project was to develop a guideline for the heat staking machine operation settings by characterizing the heat staking application currently utilized by Autoliv. This will help Autoliv optimize their present and future applications of the heat staking process. To create this guideline, experiments were conducted to closely examine the effect of variations in machine operation settings on the strength and

visual quality of the heat staked joint. The effects of failing to adhere to the specified guidelines were identified and investigated. Another goal of the project was to specify a visual quality criterion relating to the presence of flash.

1.6 Scope

While there were many aspects of the heat staking process that affect the quality of the heat stake joint, the project only investigated select parameters. The configurable machine parameters were exclusively examined. These parameters are discussed in Section 2.1.

2 Project Methodology

2.1 Parameter Selection

The quality of a heat stake joint is characterized by its strength under tensile loading, the amount of flash present, as well as the completeness of the punch print on the heat stake dome. The joint quality is dependent on both the product parameters and the process parameters. Product parameters are geometric properties of the heat stake posts, including post diameter, height, height to diameter ratio, post type (hollow v.s. filled center), and the size of the hole in the circuit board. Process parameters are related to the heat staking machine operation settings. Through consultation with the heat stake equipment manufacturer: Extol, four process control parameters were determined to have a possible effect on the heat stake joint quality. The four associated process parameters included: Heating Time, Punch Pressure, Punch Time and Air flow Rate.

The thesis project investigated the effect of variations in the process parameters to both the heat stake joint strength and visual quality. Product parameters were excluded from the scope due to the impracticalities associated with varying product parameter types. Creating samples with geometrical variations would require modifications or remanufacturing of the tooling cavities used in the production of module housings. This option was infeasible as it would greatly increase the time and costs associated with testing. Although the post height could be adjusted by machining, this option was also impractical as it would add the potential for inconsistency among machined samples. Due to the small size of the heat stake posts (approximately 2mm in diameter), computerized

numerical control machining was the only option to accurately machine the samples. However, this option was out of the range of the specified budget for the project, and so the option was not pursued. Due to issues related to cost and time, the investigation of the effects of variations in product parameters to the heat stake joint quality were not included in the scope.

2.2 Establishing Boundary Conditions

The initial step of the investigation was the determination of the boundary conditions of the four selected process parameters. The boundary values of the process parameters were established through aid from Autoliv’s engineering team as well as preliminary testing. The lower limit boundary for each of the selected process parameters was established by observing the values at which the heat stake head began forming. The upper limit boundaries of punch pressure and air flow rate were set at the maximum capacity of the heat staking machine. The upper limit boundaries of heating time and punch time were constrained by a total cycle time of 13 seconds³ to create one heat stake module. The final boundary values of the process control parameters are summarized in Table 2-1.

Table 2-1 Boundary conditions of selected process parameters

	Heating Time (s)	Punch Pressure (psi)	Punch Time (s)	Air Flow Rate (SCFH*)
High	4	50	3	50
Low	6	70	6.5	75

* SCFH – Standard cubic feet per hour

2.3 Design of Experiments

Design of Experiments (DOE) is a structured, organized method for determining the relationship between control factors (X_i) affecting a process and the output response of that process (Y)⁴. The process transforms one input signal into one measurable output signal⁵. DOE analysis can identify the important control factors which have significant effects on the output results⁶. More importantly, it quantifies the effects of these important control factors to the output response as well as the effects of interactions between control factors. The DOE analysis provides a relationship which can be optimized to determine the setting of control factors at the optimized response.

The input signal is defined as a pre-heat staked post on the module housing. The signal undergoes the process of heat staking, which transforms it into a heat staked joint (output signal). The output response is defined as the quality of the heat stake joint which can be characterized both quantitatively and qualitatively. The quantitative aspect of the output response is the tensile strength of the heat stake joint, which is measured in Newtons. The qualitative aspect of the output response refers to the visual quality of the heat stake joint. Good visual quality is to be defined (after analysis) as a specified amount of flash present around the circumference of the heat stake, and as the completeness of the punch print on the heat stake dome. To optimize the visual quality, it is necessary to quantify the amount of flash surrounding the dome circumference with a scalar measuring system defined as the Visual Quality Rating. Figure 2-1 illustrates the

P-diagram which summarizes the relationship between the input signal, the process, the control factors and the output response.

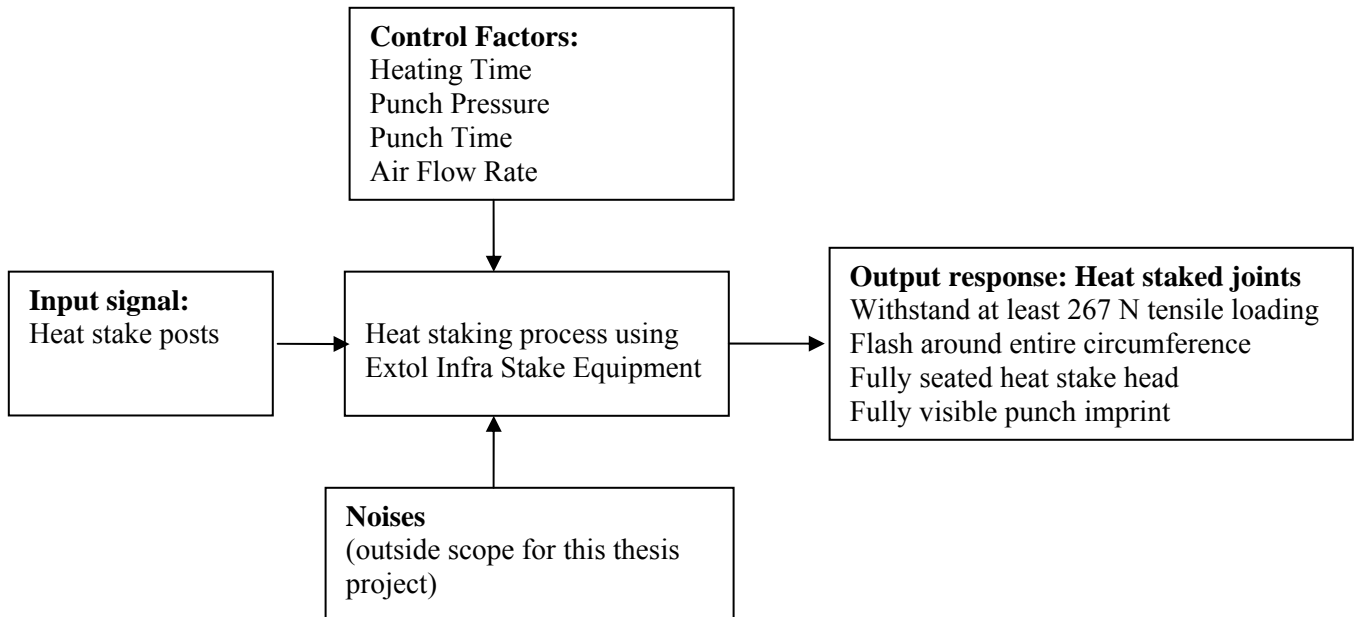


Figure 2-1 P-Diagram of heat staking process

2.3.1 Response Equation

The range of values for each control factor is partitioned into finite intervals called levels. For each experimental trial in the DOE, a distinct combination of the control factor levels is tested. For example, a full factorial DOE investigates all possible unique combinations of levels of the process parameters. The analysis of DOE quantifies the effects of control factor variations on the output response (Y) using a predictive equation of the form: $Y = F(X_1, X_2, X_3, X_4, \dots, X_n)$, where n is the total number of control factors.

For the study of four control factors, the output response Y is related to the control factors X_i in the form of following equation:

$$Y(X) = AX_1 + BX_2 + CX_3 + DX_4 + EX_1X_2 + FX_1X_3 + GX_1X_4 + HX_2X_3 + IX_2X_4 + JX_3X_4 + KX_1X_2X_3 + LX_1X_2X_4 + MX_1X_3X_4 + NX_2X_3X_4 + OX_1X_2X_3X_4 + \text{Const.}$$

A, B, C, D are the coefficients of the main effects (the standalone effect of each control factor⁷). E to O are coefficients of the interaction effects (the combined effect of two or more control factors⁸). For example, the term X_1X_2 represents the interaction effect of control factor X_1 and X_2 .

The coefficients and the constant in the above equation can be determined by performing the DOE analysis by means of statistical software. In this thesis project, Minitab was used for both the DOE design as well as the post experiment DOE analysis. The constant and coefficients of the response function were determined by running a factorial fit analysis in the Minitab.

Once the function $Y = F(X_1, X_2, X_3, X_4)$ is determined, the output response Y can be optimized by a mathematical model solver. The mathematical solver determines the values of control factors X_i that contribute to the optimum Y value. This can be achieved by use of the optimizer function in the Microsoft Excel software. In the mathematical model, the response output Y is set to be maximized while the control factors X_i are subjected to constraints corresponding to their upper and lower boundary values. The optimizer solves for the X_i values through an iterative process.

2.3.2 Justification of Utilizing the Design of Experiments Method

There are several advantages to selecting the DOE method. Any changes in the quality of the heat stakes resulting from variations in one or more process parameters can be conveniently monitored using the response equation. Through the selection of unique experimental trials, the entire spectrum of machine settings can be probed efficiently. Without DOE, the costs associated with physically changing the machine settings quickly escalate as the number of samples required is much larger. Additionally, the application of DOE and the optimization analysis serves as a guideline for Autoliv's future application of the heat staking process. If the criteria of heat stake quality are altered to meet new customer requirements or industrial standards, optimum heat staking machine parameter settings can be easily determined by re-solving the response equation. The DOE method permits an effective, and economical investigation.

There are various types of DOE each aimed to solve different problems. Often there is a trade-off between the accuracy of results and the costs⁹. The following section gives an overview of the different types of DOE and the selected approach chosen for this project.

2.3.3 Full Factorial Design of Experiments

A full factorial design of experiments can examine all possible combinations of control factors at the levels tested. It is capable of determining coefficients of the main effects of the factors as well as any interactions associated with the output response¹⁰.

The total number of experimental runs required for a full factorial DOE is determined from the following relation¹¹:

$$\text{Number of runs} = L^k$$

L is the number of levels of the design and k is the number of control factors. For a four-factor-two-level full factorial DOE, the total required number of runs to be conducted is sixteen. By increasing the number of levels, the number of experiments required increases considerably. Resource limitations inhibit the use of a full factorial experiment with more than two levels. Constraints associated with production line availability, as well as materials were the main limiting factors restricting the number of experiments that could be performed. A more detailed explanation is provided in Section 2.4.3.4.

2.3.4 Fractional Factorial Design of Experiments

Fractional Factorial DOE prescribes that only a fraction of the full factorial experiments are conducted. This can effectively reduce the number of experimental runs, allowing more factors or levels to be investigated with less time and cost. However, the savings in time and cost comes with the sacrifice of losing information about the relationship between the control factors and the output response¹². The number of experiments required in a fractional factorial DOE is described by its “fraction”. For example, a Half-Fraction DOE requires half the number of runs of a full factorial DOE and a Quarter-Fraction DOE requires one quarter of the number of runs of a full factorial DOE. The smaller the fraction, the more information that is lost.

The loss of information begins at the highest order interaction effects, and works down towards the main effects as the resolution is decreased. The term resolution describes the degree to which the main or interaction effects are confounded with other main or interaction effects. This means there is a risk that the determined main effects or interaction effects are inaccurate because there is not enough information to distinguish them from other effects. For a system where interactions contribute significantly to the output response, there exists a higher risk that a low resolution fractional factorial DOE would be inaccurate. The accuracy achieved in capturing the behaviour of a system is inversely proportional to the amount of resources required.

An L9 orthogonal array is a type of DOE which requires nine experiment trials. It is able to evaluate four factors at three levels if there are no interaction effects occurring¹³. This DOE can approximate a non-linear relationship with three points of information¹⁴.

2.3.5 Experimental Strategy Selection

Due to the resource and time constraints which include: the quantity of housings and circuit boards, and duration of production line downtime, the number of experimental runs should be minimized. Careful design of DOE can lead to extraction of meaningful information while minimizing the number of runs.

A four-factor-three-level full factorial DOE requires a total of eighty-one experiments. This larger number of experiments is infeasible due to the cost and time

constraints mentioned above. Since the four control factors are mechanical processes, it was suspected that there were no significant interaction effects between the factors.

A four-factor-two-level full factorial DOE requires a total of sixteen experiments. However if there is a curvilinear relationship between the output response and the control factors, the two-level analysis will not reveal the curvature accurately¹⁵. The curvilinear relationship is approximated with a linear relationship¹⁶. This means the analysis will not be accurate if the output result is not linearly proportional to the value of control factors. This four-factor-two-level full factorial DOE will be used to validate the non-existence of interaction effects and to determine the linear approximations of the main and interaction effects. If interaction effects do not exist then a subsequent L9 orthogonal array can be run to determine the curvature of the main effects.

A center point analysis experiment was performed along with the four-factor-two-level full factorial DOE to verify if there would be curvature relationships between control factors and the output response. A center point analysis is one additional experiment that is performed at the mid-level values of all control factors¹⁷.

The total number of runs for the L9 array, four-factor-two-level full factorial DOE, and center point analysis is twenty-six experiments. With the assumption that there are no interaction effects amongst the control factors, this DOE strategy is able to:

- Investigate the main effects of the control factors on the output response.

- Investigate if there is a curvature relationship between the control factors to the response.
- Validate the existence of interaction effects.

The most important advantage of this DOE strategy is the reduced number of experiments from 81 to 26, as opposed to a four-factor-three-level full factorial DOE. The amount of time and cost associated with the DOE method is considerably reduced while sufficient, and meaningful information about the relationship between control factors and the output response is extracted from the experiments.

2.3.6 Designed Experiments

This thesis project utilizes Minitab as the statistical software for the DOE design and analysis. Inputting the type of DOE and the boundary conditions allows Minitab to formulate the design of experiments. The table of values for the four-factor-two-level full factorial with center point and L9 array experiments are found in Table 2-2 and Table 2-3.

Table 2-2 Two level full factorial DOE with center point

Experiment No.	Control Factors			
	Punch Pressure (psi)	Heating Time (s)	Punch Time (s)	Air Flow Rate (SCFH)
1	50	4	3	50
2	70	4	3	50
3	50	6	3	50
4	70	6	3	50
5	50	4	6.5	50
6	70	4	6.5	50
7	50	6	6.5	50
8	70	6	6.5	50
9	50	4	3	75
10	70	4	3	75
11	50	6	3	75
12	70	6	3	75
13	50	4	6.5	75
14	70	4	6.5	75
15	50	6	6.5	75
16	70	6	6.5	75
17	60	5	4.75	62.5

Table 2-3 L9 array DOE

Experiment No.	Control Factors			
	Punch Pressure	Heating Time	Punch Time	Air Flow Rate
1	50	4	3	50
2	50	5	4.75	62.5
3	50	6	6.5	75
4	60	4	4.75	75
5	60	5	6.5	50
6	60	6	3	62.5
7	70	4	6.5	62.5
8	70	5	3	75
9	70	6	4.75	50

2.4 Tensile Strength Testing

2.4.1 Sample Generation

The four-factor-two-level full factorial and L9 array of designed experiments provided a specified set of trials to be conducted on the heat staking machine. These trials represented the spectrum of machine process parameter settings that were to be investigated. Table 2-2 and Table 2-3 show the corresponding parameter settings for each respective trial. This convenient set of “design tables” was used as the reference for building samples using the heat staking machine. The raw materials used to generate each sample module were an empty housing and a circuit board, which is the same as those used to make a central control module. Each central control module contains six heat stake joints. The quantity of raw materials required was determined from the total number of runs specified from the four-factor-two-level full factorial, and the L9 array in addition to requirements for early testing and verification of settings. Their quantities are detailed in Table 2-4.

Table 2-4 Raw materials required to run trials

Raw Materials	Quantity Required	Description/Notes
Empty Module Housings	30	Pulled from excess inventory
Individual Circuit Boards	30	Routed from 8 motherboard panels

The following subsection describes the steps that were required to generate sample heat stake joints using the heat staking equipment.

Step 1: Circuit Board Preparation

A circuit board must be placed in the plastic housing prior to the heat staking operation. Although the circuit board was an extra expense that would have ideally been avoided, it played a critical role in the heat staking process for the following reasons. As seen in Figure 2-2, when the punch head extends down to compress the semi-molten heat stake post, the flow of material is impeded by the surface of the circuit board, and compressed under the punch head. However, without the presence of a circuit board, the semi-molten plastic has no surface to impede its flow downward, and the result is a malformed head as shown in Figure 2-3. More importantly, the heat staking machine itself would not allow operation without a circuit board. It is programmed to ensure that the punch head reaches a minimum of 10 psi¹⁸ of back pressure, which cannot be reached without a circuit board.

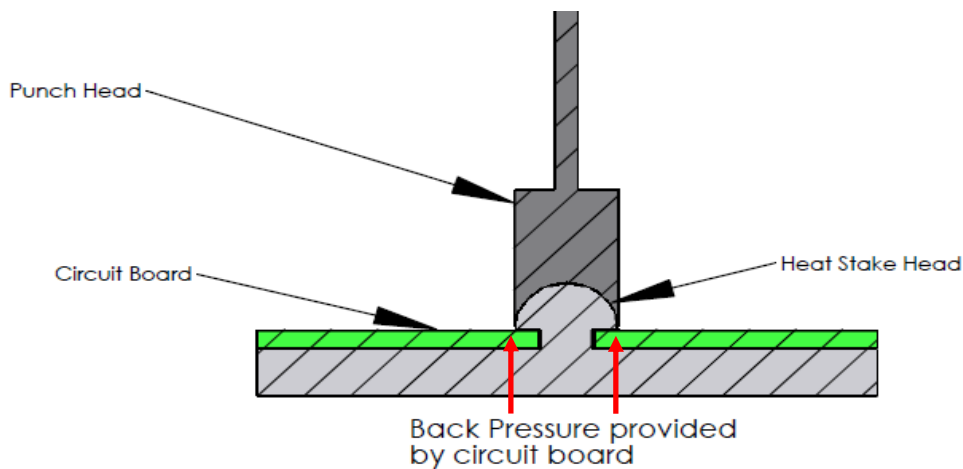


Figure 2-2 Back pressure provided by circuit board required for head formation

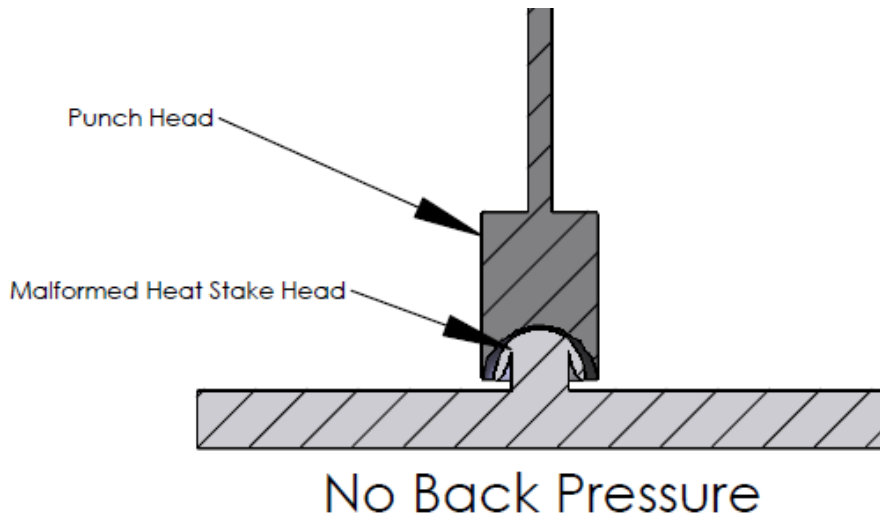


Figure 2-3 Malformed heat stake head resulting from inadequate back pressure

To minimize the expense related to the consumption of circuit boards for testing, a bare circuit board was used for sample generation as opposed to populated boards. Bare circuit boards have the exact same physical dimensions as the populated boards, but lack any of the expensive components that make up a fully populated circuit board. The use of bare circuit boards for testing was justified as electronic components on the board were spatially separated from the heat stake joint sites on the circuit board, and thus they would have no effect on the quality of the heat stake joint. This decision was an effective cost reduction measure which posed no impact on the desired test results.

The bare circuit boards were delivered to the plant in the form of mother panels as seen in Figure 2-4. The mother panels had to be separated into smaller, individual boards, called daughter-boards. The quickest and cleanest method to separate the mother panel was to use the production line's routing machine. The machine was placed into bypass mode so that it could be operated under manual conditions with special instructions. The

machine was configured to run the mother panels through the routing process, and then bypass its normal operation of placing the routed circuit board onto the final assembly dial table. Instead the machine presented each routed bare circuit board on the scrap conveyor for collection. Figure 2-5 shows a mother panel undergoing routing process. Thirty bare daughter boards were generated for experimental tests.

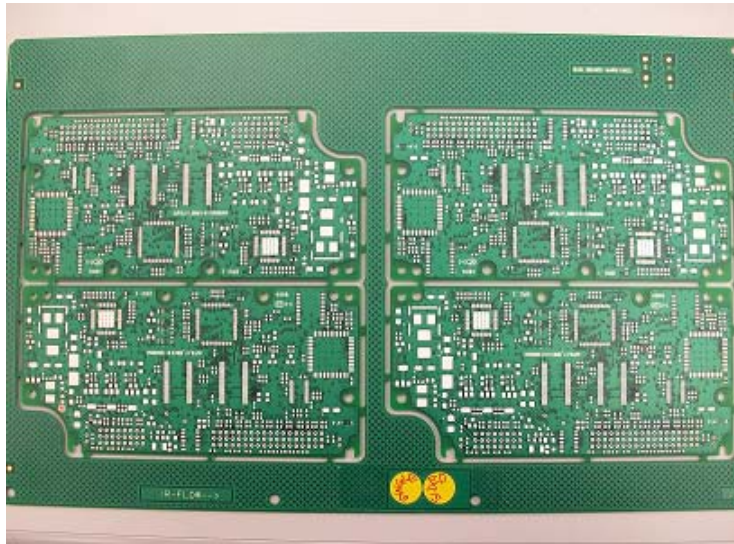


Figure 2-4 Mother panel containing four bare daughter boards

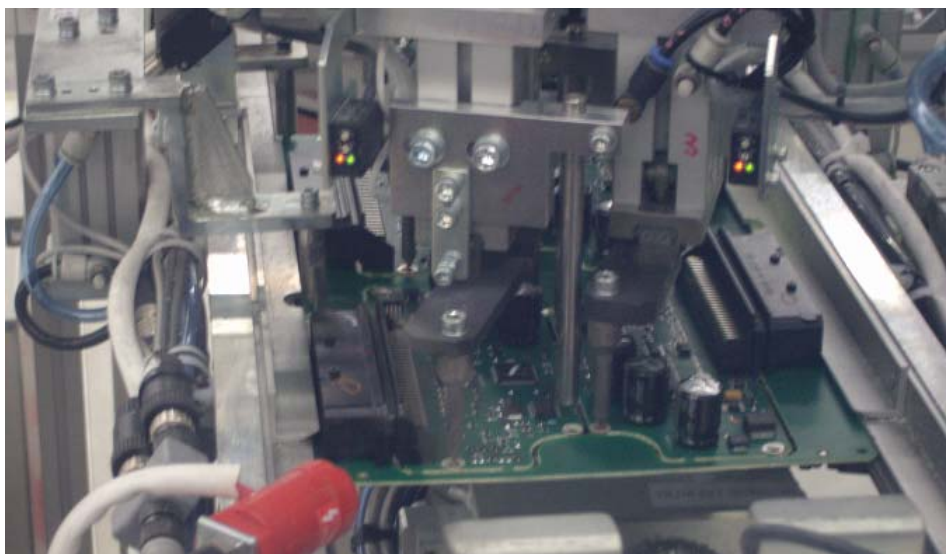


Figure 2-5 Mother panel undergoing routing process

Step 2: Pressing Circuit Boards into Housing

After all the daughter boards were created, the next step was to use the press station on the dial assembly table to mount each circuit board into the housing. The press machine was used to simultaneously insert forty-two connector pins from the housing into the circuit board. The machine was set to perform this operation at seven hundred Newtons of force.

In this step, each daughter board was loosely placed onto the connector pins while heat stake posts served as guides to locate the board in the housing. It is important to note that the press process had no contact or stress inducing effect on the heat stake posts. The heat stake posts were not press fit through their corresponding holes on the circuit board, instead they had a sliding fit interaction. The assembly was then placed into the jig under the press head, and the press machine was operated in manual mode so that the rest of the dial table stations could remain inactive.

Step 3: Run Samples under Heat Stake Machine

At this point, the individually routed daughter boards had been pressed into the housings, and the remaining step was to form the heat stake joints. Prior to heat staking, the heat staking machine was programmed to run in a “dry cycle” mode. This mode enabled the heat staking machine to run its normal heat staking functions while being isolated from the rest of the dial table. This ensured the dial table would not rotate and begin the next step in the assembly process. The heat staking machine was then operated

to form heat stakes. After running the samples through the heat staking process, they were ready for inspection and tensile testing as outlined in Section 2.4.3.

At this stage, the set of designed experiments played a major role in specifying the setup of the heat staking machine for generating each sample. Each run in the experiment consumed one module, which consisted of one housing and one daughter board. The sequence of steps performed for each experimental trial is detailed below:

- 1) Read settings for Heating Time, Punch Time and Punch Pressure from the experiment design table, and entered them into the control panel.
- 2) Read settings for Air Flow Rate from experiment design table, and adjusted valves until gauges displayed the desired setting.
- 3) Placed pre-heat staked module into jig, and started “dry cycle”.
- 4) Removed module from the fixture and inspected it for damage once the cycle completed.
- 5) Repeated the process for next trial in experiment design table until all trials were completed.

This process was followed for each of the twenty-six experiments, and then the machine was returned to its current production settings and tested to verify that it was operating to current production standards. Figure 2-6 shows the heat staking machine and the surrounding dial table machinery. Figure 2-7 shows the six heat stake nozzles that

were used to form the heat stake joints. The green arrow indicates the placement of a module.

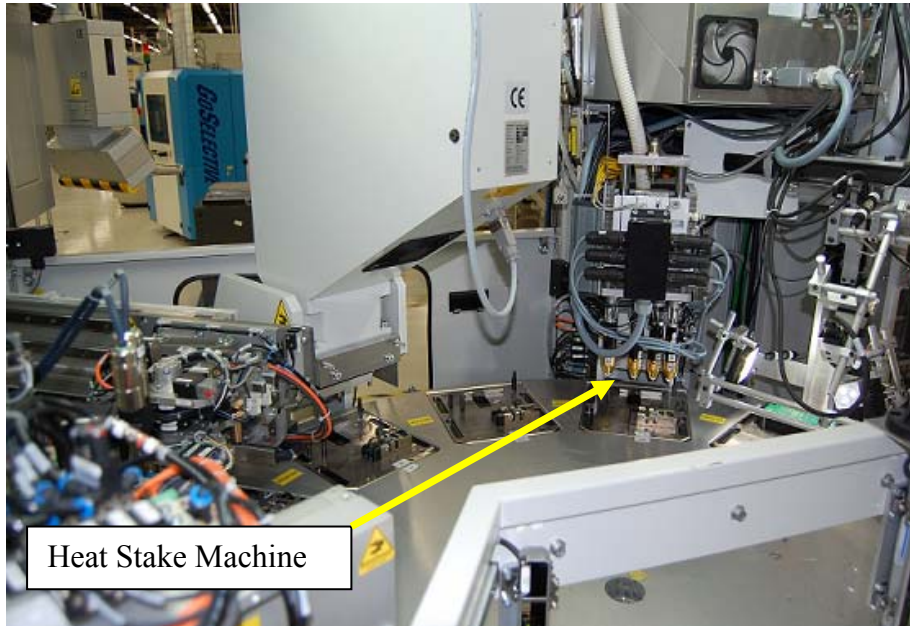


Figure 2-6 Heat staking machine within the assembly dial table

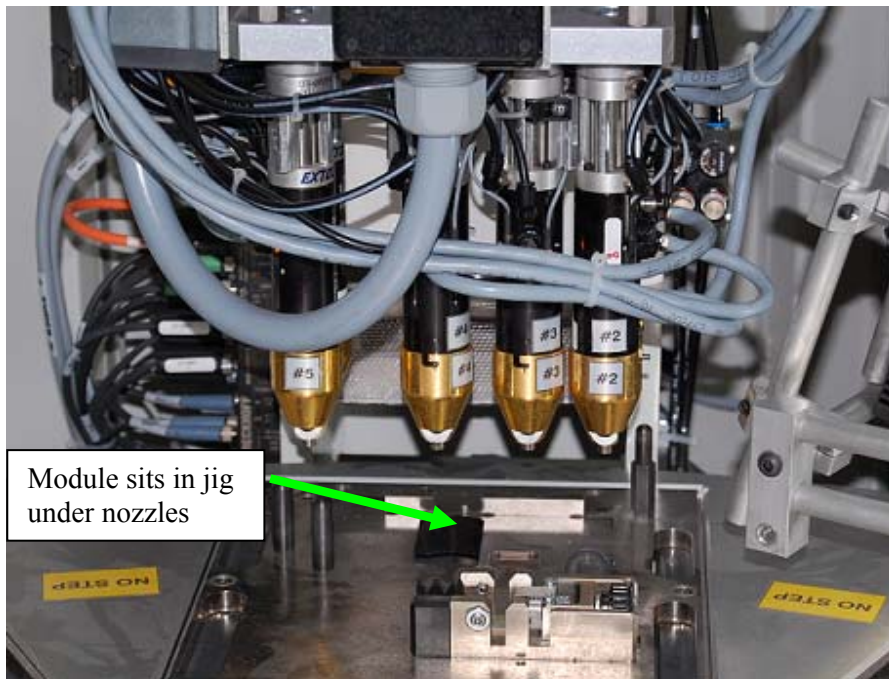


Figure 2-7 Close-up of the heat staking nozzles

2.4.2 Visual Data Acquisition

After sample generation at Autoliv, each sample module was photographed for visual analysis. This was required because the samples would eventually undergo destructive tensile testing, thus inhibiting any subsequent form of heat stake visual quality investigation. Section 2.4.3.2 is a description of the destructive testing procedure.

A high resolution, visual quality reference image of each module sample was recorded and catalogued according to the experimental trial number. This made it convenient to refer to the samples at any time during the analysis. Figure 2-8 is an example of a visual quality reference image, and it presents the numbering system used to keep track of each heat stake's orientation within the module. These reference images were used to inspect, and quantify different aspects of the visual quality of each heat stake joint. Table 2-5 lists the visual quality metrics that were used in the investigation.

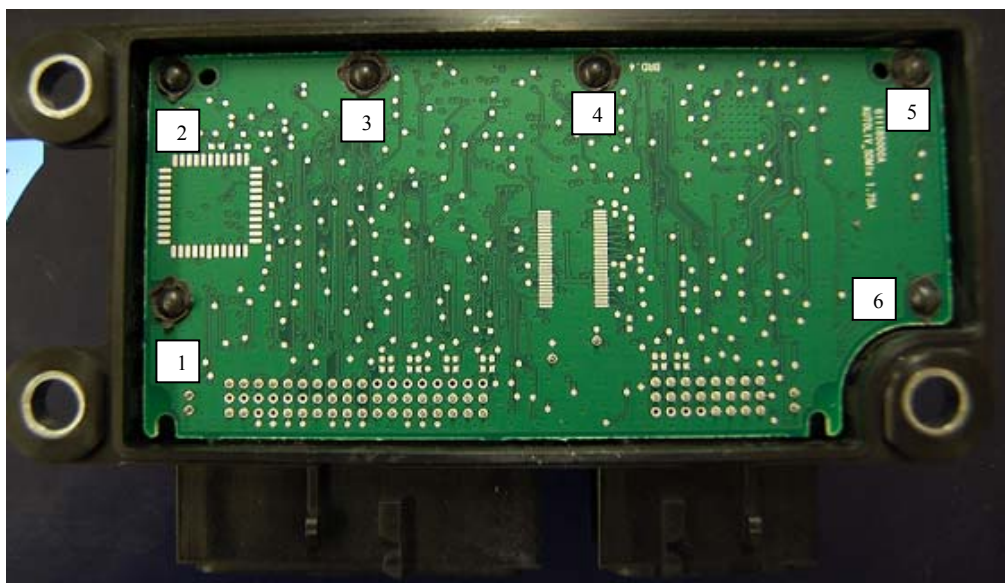


Figure 2-8 Reference visual quality image

Table 2-5 Visual quality metrics used in visual analysis

Visual Quality Category	Metric
Incomplete Joint(malformed head)	# of Instances (0-6)
Presence of flash	Yes/No
Quantity of flash present	Scale Rating (0-10)*

*To quantify the amount of flash present, a scale was used to represent the fraction of flash coverage to the circumference of the heat stake head. For example, a rating of five represents fifty percent flash coverage around the heat stake head circumference. The Photoshop application was used to accurately measure the angle of flash coverage. Figure 2-9 illustrates the measurement process.



Figure 2-9 Measurement of flash on heat stake head

By obtaining the angle of flash coverage, the percentage of flash coverage can be calculated, and multiplied by ten to give a corresponding scale from zero to ten; zero indicating no flash present, and ten indicating full flash present around the circumference of the heat staked head.

The following equation shows the formula used to calculate the rating for quantity of flash present.

$$Flash_{present} = \frac{Flash_{coverage}(\text{deg})}{360(\text{deg})} \times 10$$

The results of the visual data acquisition and analysis are listed in Section 3.3.

2.4.3 Tensile Testing Experiment

To establish the relationship between the machine settings and the strength of the heat stake joint, the failure strength of each joint had to be quantified through tensile testing. The results were then analyzed through techniques outlined in Section 3.

2.4.3.1 Extraction of Heat Stake Joints

Each sample control module contains six individual heat stakes that are moulded into the plastic housing. Figure 2-10 shows that the heat stake joints and their bases are contained inside the housing and under the circuit board. Each joint required extraction from the housing prior to tensile testing.

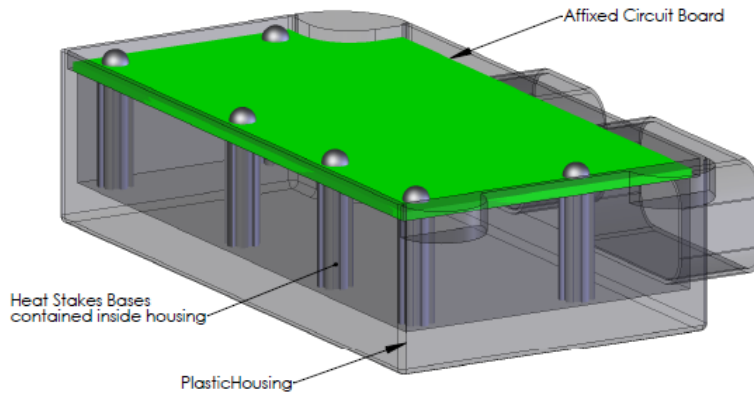


Figure 2-10 Heat stake base locations within the module

This heat stake joint extraction process required cutting and other finishing operations to gently separate the heat stakes and their bases from the module without inducing stress on the joints. The process was complicated due to the highly brittle nature of the fibreglass circuit board. High speed cuts were made with a sharp carbide tipped band saw to avoid cracking and inducing excess stresses on the board. Figure 2-11 shows the cutting planes (blue in colour) that were used on the module.

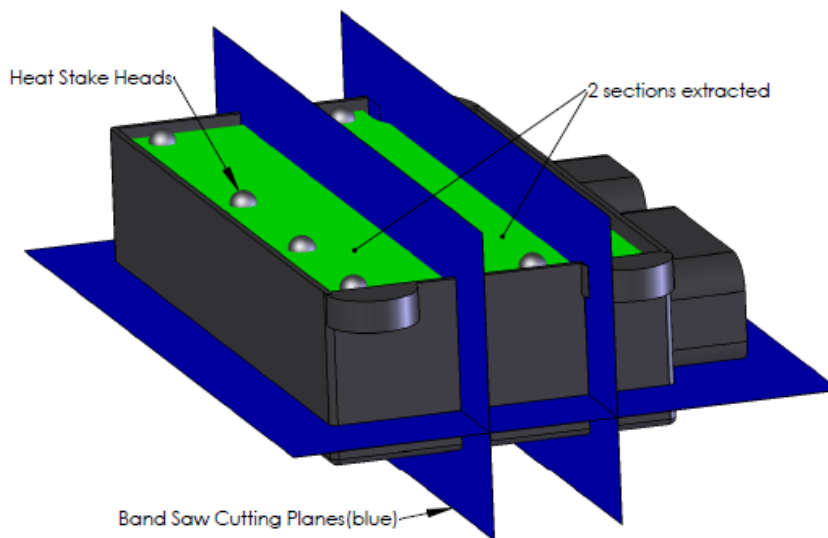


Figure 2-11 Cutting planes used to extract the heat stakes

Despite precautionary cutting measures mentioned above, heat stake joints were often broken in early process testing. This problem was solved by placing wooden blocks underneath the circuit board to support the heat stake joint from the forces induced by the band saw blade. This eliminated the moment loading on the joint and dampened the vibrations. The orientation of the load previously induced on the joint and the position of the wooden blocks in the housing are shown in Figure 2-12.

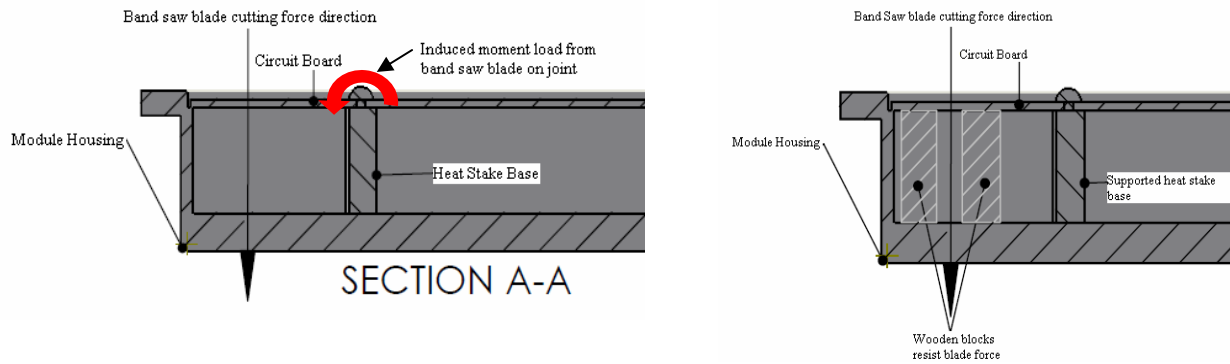


Figure 2-12 Induced loads during cutting operation

Heat stake joints that have been extracted are depicted in Figure 2-13 below.

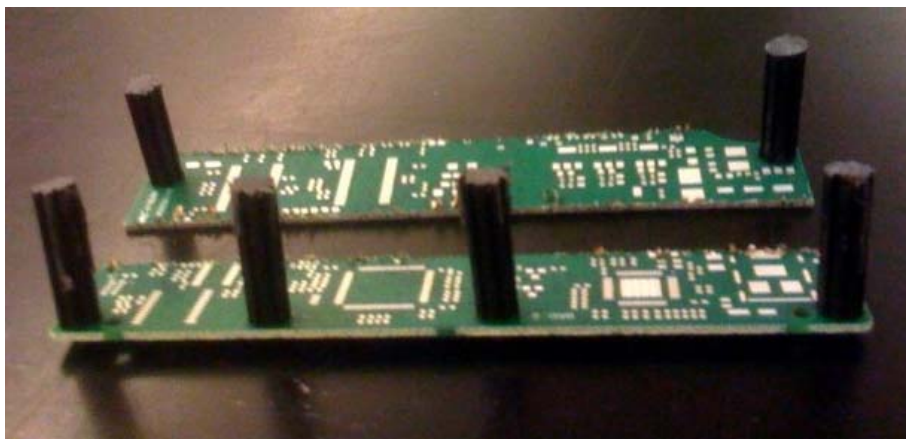


Figure 2-13 Heat stakes extracted from the module

2.4.3.2 Tensile Testing Experiment Method

Two methods were proposed to evaluate the failure strength of each joint:

- Failure Testing with Calibrated Weights
- Failure Testing using Instron Tensile Testing Machine

A brief discussion of the two options and selection of methods follows.

Method 1: Failure Testing with Calibrated Weights

This method was initially proposed as it seemed to be the simpler option. Since only the failure strength of the joint was required for analysis, this method would have accomplished the task. However during early process testing many flaws and setbacks were encountered. Sequentially incrementing the test load until failure for each sample was time intensive. Additionally, it was challenging to maintain the experimental conditions between different test runs. One such issue was manually adding weights to maintain the strain rate (mm/min) as specified by Autoliv (2mm/min)¹⁹. A schematic and image of this method in progress is depicted in Figure 2-14.

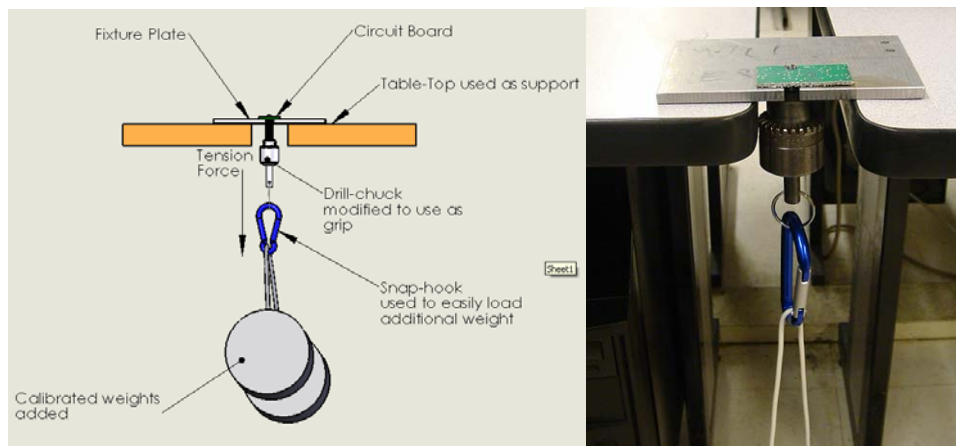


Figure 2-14 Preliminary tensile testing method: manual loading

Method 2: Failure Testing Using Instron Tensile Testing Machine

This method utilized the Instron tensile testing machine in the Solid Mechanics Laboratory at the University of Toronto. The Instron machine includes data acquisition software and has a load measurement resolution of 0.1N, which was read from the machine data output. There were several features of the machine that were critical to the accuracy and repeatability of the test results. One of these features was the ability set the strain rate of the tensile loading, to match the Autoliv standard (2mm/min). Another convenient feature was the data logging software which recorded the maximum force before failure. As a result, the Instron machine was selected as the method of tensile testing due to better repeatability, accuracy, and convenience over the calibrated weight testing method.

2.4.3.3 Customized Hardware

A customized fixture was required to test heat stake samples in the Instron machine. The fixture accounted for the irregular geometries of the heat stake samples. As seen in Figure 2-15, without any fixture, the tensile machine's bottom claw can easily clamp onto the base of the heat stake, however the top claw is only able to clamp onto the fragile circuit board. It would be difficult to maintain the circuit board in a level horizontal position, and thus results may be skewed due to asymmetrical loading. Inducing this clamping force onto the circuit board itself may cause failure prior to the heat stake joint failing, which would provide no meaningful data from the test.

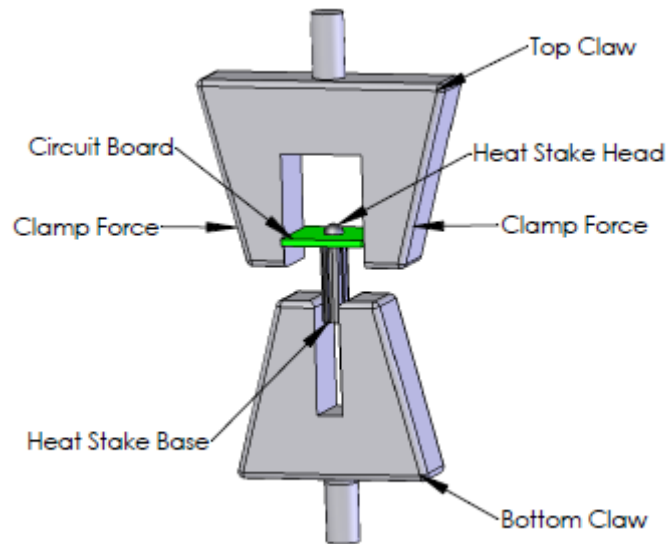


Figure 2-15 Clamping the heat stake sample without a fixture

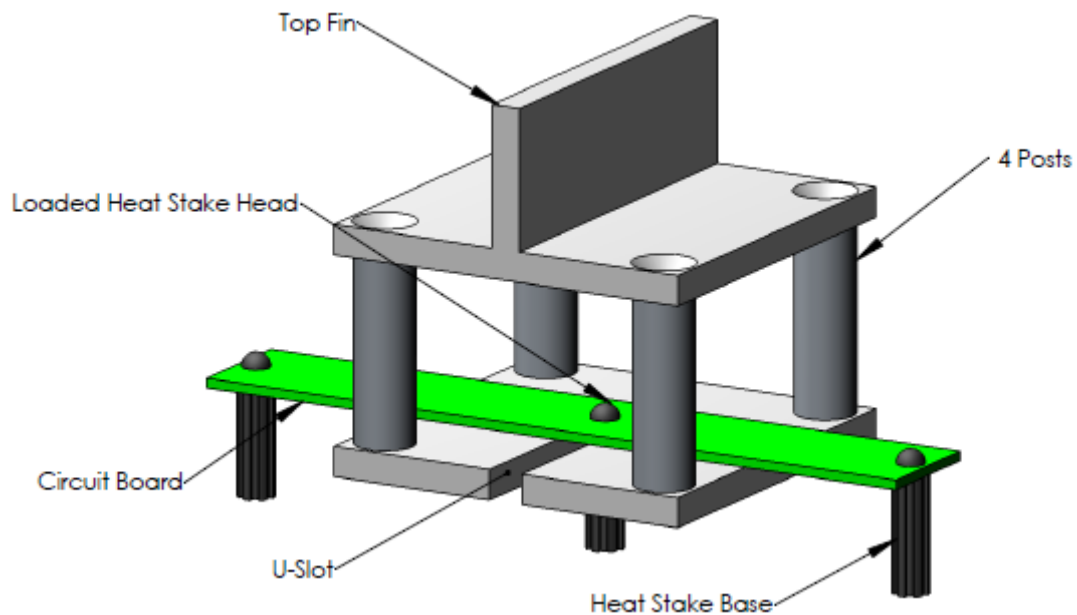


Figure 2-16 Design of the tensile test fixture

The test fixture is the assembly depicted in Figure 2-16. The design has several characteristic features, one being the top fin, which is the surface that the top claw could grip onto, and load in an upward direction. The precision milled “U-slot” allows quick

loading, and unloading of the heat stakes into and out of the fixture. It is designed to have a sliding fit interaction with the heat stake post. The slot fit ensures that the circuit board will not deflect downward during loading and cause premature failure. The fixture has a post on each of the four corners so that large heat stake samples can be accommodated (see Figure 2-16) while the overall footprint of the fixture remains relatively small. The fixture was symmetrically dimensioned so that during testing, no asymmetric loading would be induced.

Figure 2-17 depicts the orientation of the forces that load the sample. Figure 2-18 shows the fixture in the tensile machine while a sample is being tested. The fixture increased convenience to mount and dismount samples into the machine, and ensured the samples were consistently loaded in the appropriate orientation. Using this fixture reduced setup time for each trial, and ensured samples were consistently loaded in the desired orientation.

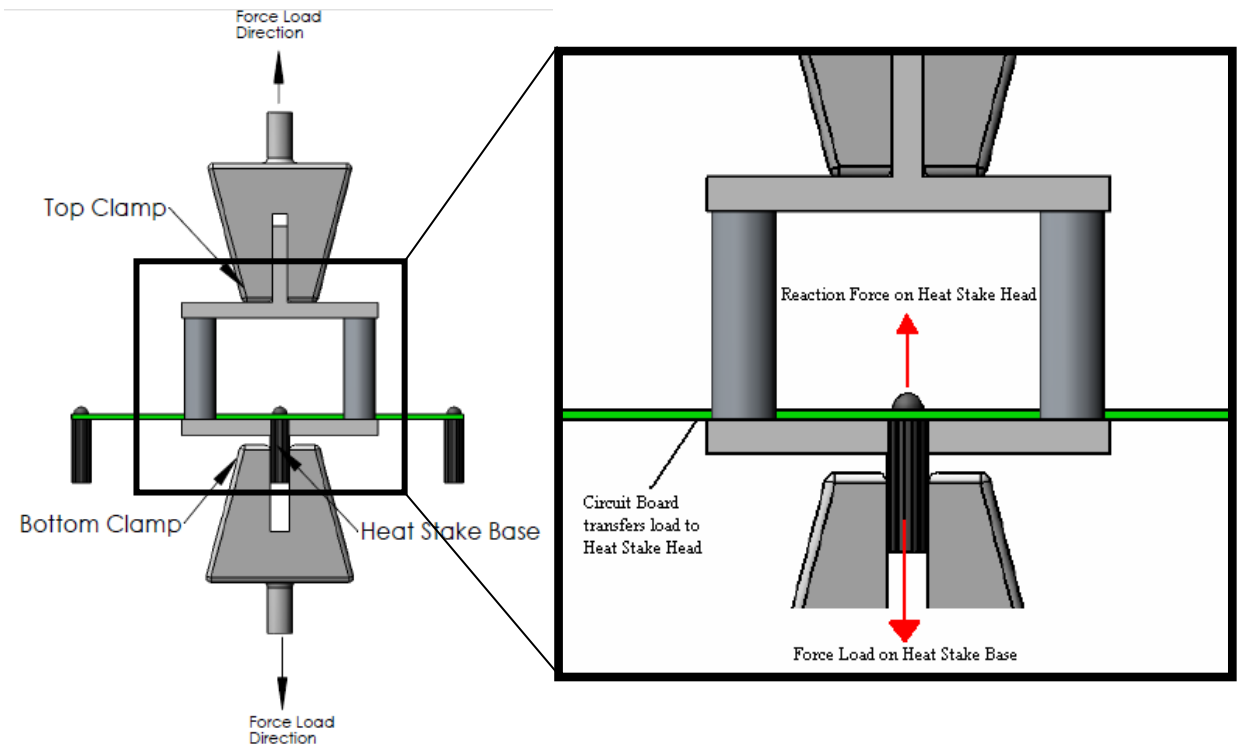


Figure 2-17 Force loading on a heat stake sample for the selected fixture



Figure 2-18 Heat stake sample testing in Instron Machine

2.4.3.4 Financial Breakdown: Costs Related to Experiments

This section focuses on the cost typically incurred by a company such as Autoliv if it were to pursue this investigation through a consultant or other industrial professional.

The costs can be separated into three distinct areas:

- Material/Equipment Costs
- Consultation Costs
- Line Downtime

Material and equipment costs included the raw components consumed for testing. This is comprised of the plastics housings, the bare circuit boards, as well as the costs related to the use of the tensile testing equipment.

Consultation costs typically stem from the company contracting a consulting firm, or engineers to investigate a problem at hand. In this project the students held this role but these costs were included for future reference in the event the company needs to evaluate the feasibility of another study. For this analysis it was assumed a junior consultant, and a senior consultant shared the investigation. Typically, a junior and senior consultant's fees would be \$70 and \$140 per hour respectively²⁰. The estimated time spent on the project by the consultants is based approximately on the time that it would take students to complete the study less the research and understanding period. The time derived from this assumption was one-hundred hours. It was also assumed that thirty of the one-hundred hours would be the duration of work performed by the senior consultant, and seventy hours would be spent by the junior consultant. This division of work was

based upon the hours that the junior and senior consultant would spend on each of their respective tasks. Typically, a junior consultant would focus on gathering background information and progressing forward on a direction that has been selected by the senior consultant²¹.

Costs relating to line downtime are the outcome of stopping production for the period in which experiments are performed. The design of experiments method used in this investigation was instrumental in reducing the line downtime by minimizing the number of tests necessary to extract a meaningful result. It is important to note that the production line was previously scheduled for a production stoppage as per Autoliv's standard schedule. The tests were conducted during this pre-scheduled stoppage to eliminate the cost of downtime related to the project. However, it is included in the analysis to account for any future investigation for which production stoppage might not be avoidable. Table 2-6 summarizes the costs discussed above.

Table 2-6 Financial breakdown for heat stake investigation

	Unit Cost	Quantity	Total Cost
Material Costs			
Plastic Housings	\$5/housing	30	\$150.00
Mother Panels (Circuit Boards)	\$8/panel	8	\$64.00
Consultation Costs			
Jr. Consultant*	\$70/hour	70	\$4,900.00
Sr. Consultant*	\$140/hour	30	\$4,200.00
Downtime Costs			
SDM-10 Line Downtime*	\$11000/hour	2	\$22,000.00
Total Experiment Cost			\$31,314.00

* These estimates were not incurred for this project, but included for future cost analysis.

As can be seen from Table 2-6, line downtime has the largest contribution to the overall cost of the investigation. DOE methods can considerably minimize this downtime cost.

3 Analysis of Results

3.1 Results Overview

The core of the result analysis lies in extracting the relationship between the heat stake equipment process parameters and the heat stake joint strength, as well as visual quality. The first step was to identify the existence of a correlation between the heat stake's visual quality and its strength by comparing the two characteristics. As outlined in the following sub-sections, common process parameters were found to affect both the heat stake joint strength and visual quality. The existence of these common parameters suggested that there was a correlation between the visual quality and strength of the joint. The following analysis extracted that specific relationship.

In order to characterize the relationship between the process parameters to the heat stake joint strength, the first step was to enter the tabulated heat stake joint strengths (Table 3-1) into Minitab's Design of Experiments analysis. Through the analysis of means²², Minitab returned each factor's contribution to the strength in the form of an overall response equation as defined in Section 2.3.1.

To characterize the process parameters' effect on the visual quality of the heat stake joint, a similar analysis was performed by entering the visual quality data (defined as the flash coverage around the circumference of the heat stake head) into the Design of Experiments Analyze function in Minitab. From this function, a response equation was developed to characterize the process parameter relationship to the visual quality.

The final step of the analysis was to enter both the heat stake joint strength and visual quality response equations into an optimizer to determine a set of values that would both maximize the heat stake joint strength and the circumference of flash.

3.2 Heat Stake Joint Strength Results

The tensile testing results for the four-factor-two-level full factorial array with center point analysis, and the L9 orthogonal array experiments are shown in Table 3-1 and Table 3-2 respectively. The tabulated data show the failure tensile force of each of the six heat stake samples across each corresponding heat stake module.

Table 3-1 Tensile strength results for four-factor-two-level full factorial DOE with center point analysis

Module	Nozzle 1 (N)	Nozzle 2 (N)	Nozzle 3 (N)	Nozzle 4 (N)	Nozzle 5 (N)	Nozzle 6 (N)
1	413.55	278.52	211.27	308.29	270.87	388.1
2	352.21	279.06	361.87	262.81	374.36	388.32
3	452.75	469.12	346.04	377.85	401.2	412.22
4	465.1	432.61	457.44	442.28	368.85	431.95
5	467.38	197.18	435.43	230.87	252.34	491.54
6	457.18	288.45	418.82	384.69	364.56	473.42
7	466.44	444.96	460.8	471.4	303.22	413.95
8	412.23	427.91	428.32	426.3	369.26	435.83
9	457.04	161.47	240.4	332.08	269.79	396.51
10	407.51	154.49	288.99	212.61	162.01	251.27
11	489.12	441.34	433.95	407.24	343.08	442.28
12	482.41	375.43	385.23	408.45	322.81	397.31
13	412.09	153.42	224.96	301.47	233.02	418.25
14	467.11	140	233.02	153.82	224.69	409.93
15	501.74	373.82	466.17	453.28	320.53	535.83
16	540.4	433.42	399.59	425.36	377.98	466.84
17	481.07	402.95	347.65	383.89	413.58	439.46

Table 3-2 Tensile strength testing results of L9 array DOE

Module	Nozzle 1 (N)	Nozzle 2 (N)	Nozzle 3 (N)	Nozzle 4 (N)	Nozzle 5 (N)	Nozzle 6 (N)
1	438.12	283.35	420.53	190.87	271.94	402.95
2	457.71	421.47	388.59	393.69	358.52	432.61
3	484.83	496.37	360.13	324.56	337.58	442.55
4	402.41	212.75	196.37	239.32	213.69	480
5	408.32	436.1	344.16	490.46	276.51	382.81
6	470.73	461.2	312.88	414.89	351.14	431.67
7	421.34	236.1	272.61	202.95	335.83	378.92
8	395.97	335.83	273.82	287.91	389.12	430.33
9	473.82	488.05	424.42	423.35	375.16	456.1

3.3 Heat Stake Visual Quality Results

The visual quality results of the four-factor-two-level full factorial array with center point analysis and the L9 orthogonal array experiments are shown in Table 3-3 and Table 3-4 respectively. The quality is measured in scalar units as a percentage of the heat stake dome circumference surrounded by flash (see Section 2.4.2 for more details).

Table 3-3 Visual quality results for four-factor-two-level full factorial DOE with center point analysis

Module	Nozzle 1	Nozzle 2	Nozzle 3	Nozzle 4	Nozzle 5	Nozzle 6
1	0	0	0	0	0	0
2	10	5	10	4	7	0
3	10	10	10	10	8	0
4	10	10	10	10	10	0
5	7	0	8	0	4	0
6	10	4	10	5	6	2
7	10	10	10	10	8	5
8	10	10	10	10	4	3
9	0	0	0	0	0	0
10	7	0	3	0	3	3
11	10	10	10	7	6	4
12	10	10	10	6	7	4
13	2	0	0	0	0	0
14	6	0	3	0	3	0
15	10	10	10	8	8	4
16	10	10	10	7	8	4
17	10	10	10	7	8	4

*Rating Scale: 0-10

Table 3-4 Visual quality testing results of L9 array DOE

Module	Nozzle 1	Nozzle 2	Nozzle 3	Nozzle 4	Nozzle 5	Nozzle 6
1	10	0	9	0	5	4
2	10	9	10	6	10	3
3	10	10	10	7	10	3
4	4	0	4	0	3	1
5	10	7	10	10	9	3
6	10	10	10	10	10	4
7	10	0	3	1	4	1
8	10	9	10	5	9	3
9	10	9	10	9	8	2

*Rating Scale: 0-10

3.4 Visual Quality Correlation to Strength

For each heat stake sample, both a visual quality inspection and a tensile strength test were performed. This enabled a scalar measurement (rating) of the visual quality to be linked to a tensile strength for each sample. From this set of data, a relationship was examined between the instances of high heat stake joint strength and the amount of flash present at its circumference.

The 102 joint-strength data values in the four-factor-two-level full factorial experiments with center point analysis were paired with their corresponding visual quality ratings. Heat stake joint strengths were grouped according to corresponding visual quality ratings (zero to ten), and the mean and standard deviations for these grouped datasets were calculated. A plot of the joint strengths versus their respective visual quality ratings are shown in Figure 3-1.

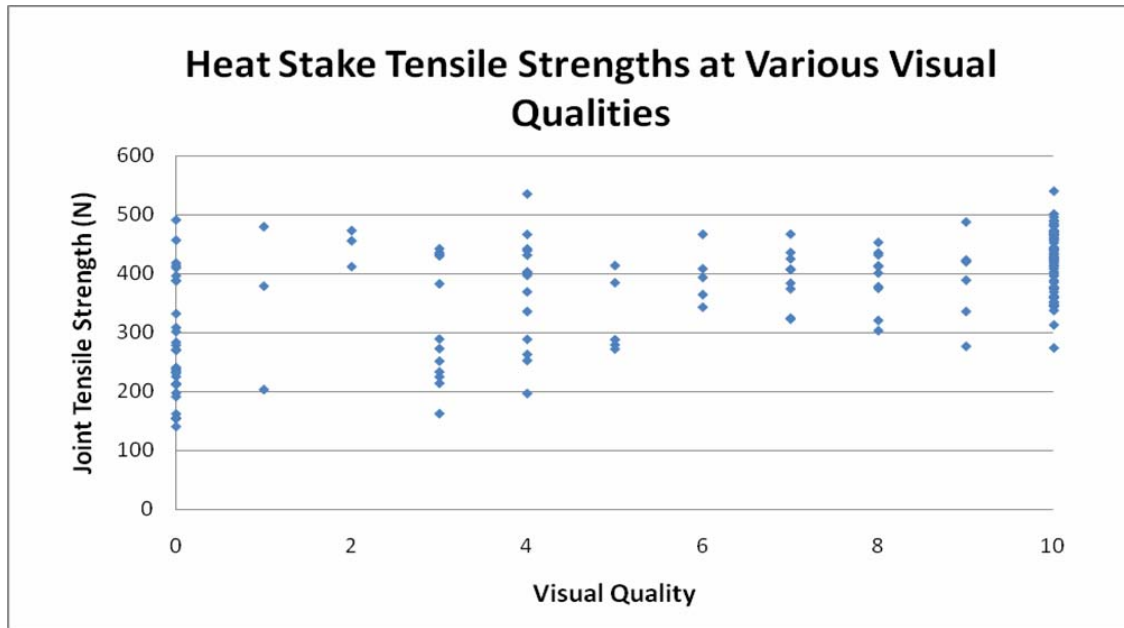


Figure 3-1 Visual quality values versus heat stake strengths

From Figure 3-1, it can be observed that at visual quality ratings of two and ten, the mean tensile strengths are highest. Since there are only three data entries at the visual quality rating of two, no meaningful conclusions can be made about a rating of two correlating to consistently high joint strengths. There is not enough information present in only three data points, and thus the true statistical distribution of joint strength is not known with satisfactory confidence.

Table 3-5 Mean and standard deviation strength for each visual quality rating

	Visual Quality Rating										
	0	1	2	3	4	5	6	7	8	9	10
Mean (N)	277.4	354.0	447.2	314.2	373.1	327.5	395.4	394.4	392.5	393.6	422.1
Stdev (N)	98.9	140.2	31.6	103.4	94.8	66.6	47.4	48.6	49.1	68.8	54.3

At a visual quality rating of ten, the mean tensile strength is higher and has lower variability (standard deviation) compared to lower visual quality ratings. A rationalization to this observation is that when flash is present around the full

circumference of the heat stake head, the head itself is more symmetric and completely formed, thus it has a higher strength. The excess flash around a heat stake dome is formed when the heat stake material has been heated sufficiently to become semi-molten and flow. Excess flash appears when the heat stake material flows out between the punches and the circuit board. The heat stake dome may not be symmetric and completely formed for the instances with lower visual quality ratings. This scenario occurs when only a portion of the heat stake post becomes semi-molten. Higher visual quality values indicate that the heat stake material has been heated more evenly to a semi-molten state and thus can be formed effectively by the punches. A more complete heat stake dome results in a higher surface area and increased symmetry and thus is able to distribute loads more evenly amongst the heat stake dome. This explains the observed trend between higher tensile strengths and higher visual quality ratings.

3.5 Heat Stake Joint Strength Analysis

The heat stake joint strength data for the four-factor-two-level full factorial array with center point analysis in Table 3-1 was analyzed using the Design of Experiments Analyze function in Minitab; the significant main and interaction effects were determined shortly thereafter.

A null hypothesis assumption²³ made by Minitab stipulates that there is a probability that the observed response values (strength data) are not related to or driven by main and interaction effects but are instead random results. If the probability of this scenario occurring is below a defined level of risk (alpha) then that main or interaction

effect is considered statistically significant²⁴. The maximum risk of concluding that a factor has a significant effect on the response when it actually does not is defined as the alpha risk value or p-level in Minitab. The alpha risk has been set as 0.05 as an industrial standard and as requested by Autoliv Electronics Canada. A Pareto chart of the significant factors can be seen in Figure 3-2.

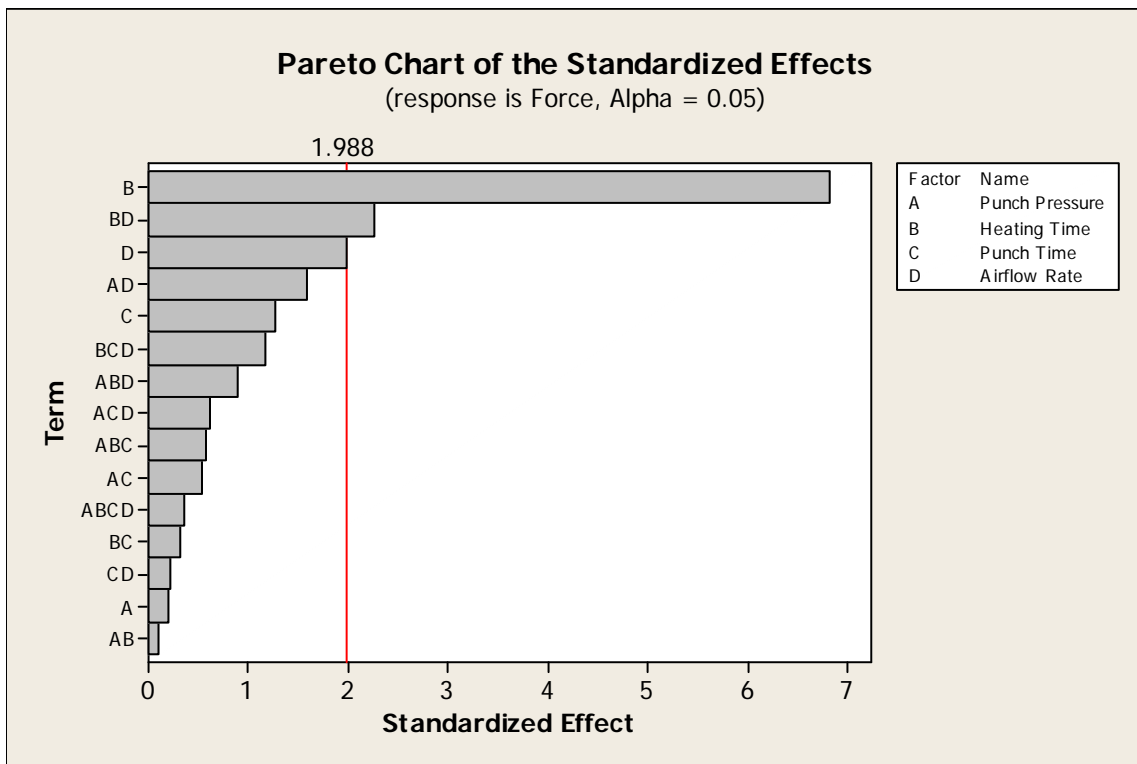


Figure 3-2 Pareto chart for heat stake joint strength analysis

The red line is where alpha risk is 0.05. Effects to the right of the line are statistically significant in contributing to the strength response with at least 95% confidence, and effects to the left of the line are considered statistically insignificant. This DOE is resolution five, meaning no second order interaction effects are confounded with other second order interaction effects. For example, interaction effect BD is not confounded with interaction effect AD, AC, BC, CD, or AB. Thus, any significant

second order interaction effects in the Pareto chart (Heating Time*Airflow rate) were not confounded with any other secondary effects. This meant that the Heating Time*Airflow rate interaction was unique. The Pareto chart shows that the significant factors to the joint strength are:

- Heating Time
- Air Flow Rate*Heating Time
- Air Flow Rate

The main effect plot is shown in Figure 3-3. The steepness of the slope is proportional to the contribution each effect has on the output response, which in this case is the joint strength. It can be seen that the Heating Time has the most significant contribution effect.

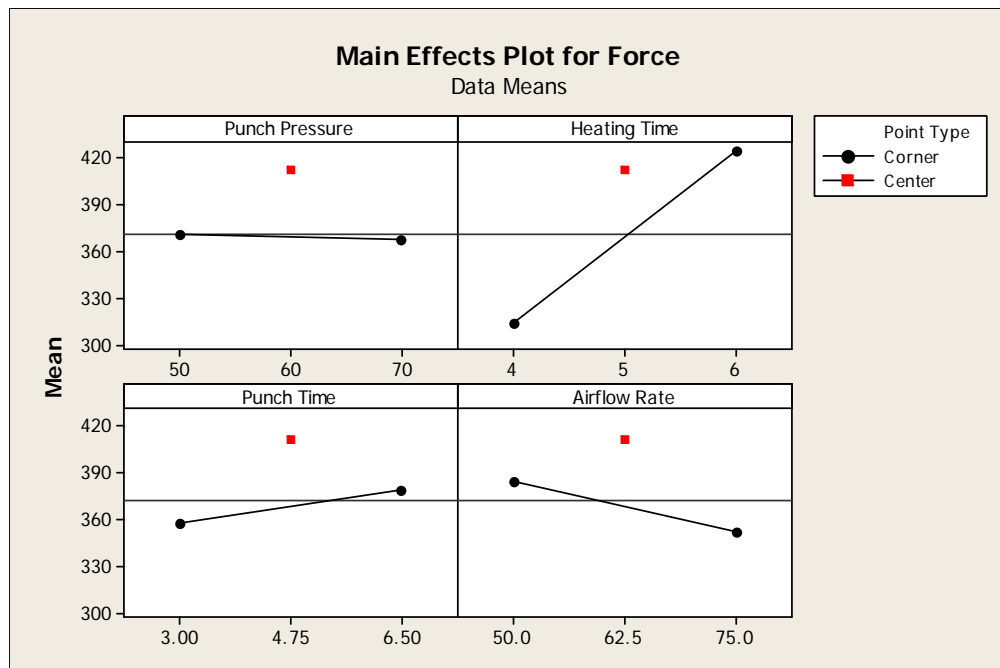


Figure 3-3 Main effect plot for heat stake joint strength analysis

The interaction plot is shown in Figure 3-4. Interaction effects which have parallel lines do not contribute to the response. Interaction effects with converging slopes have a weak contribution on the response while distinctly intersecting slopes have a substantial contribution to the response. It is important to note that these relationships only apply to the interaction effects that have alpha less than or equal to 0.05, which in this case is only the Heating Time* Airflow rate interaction effect.

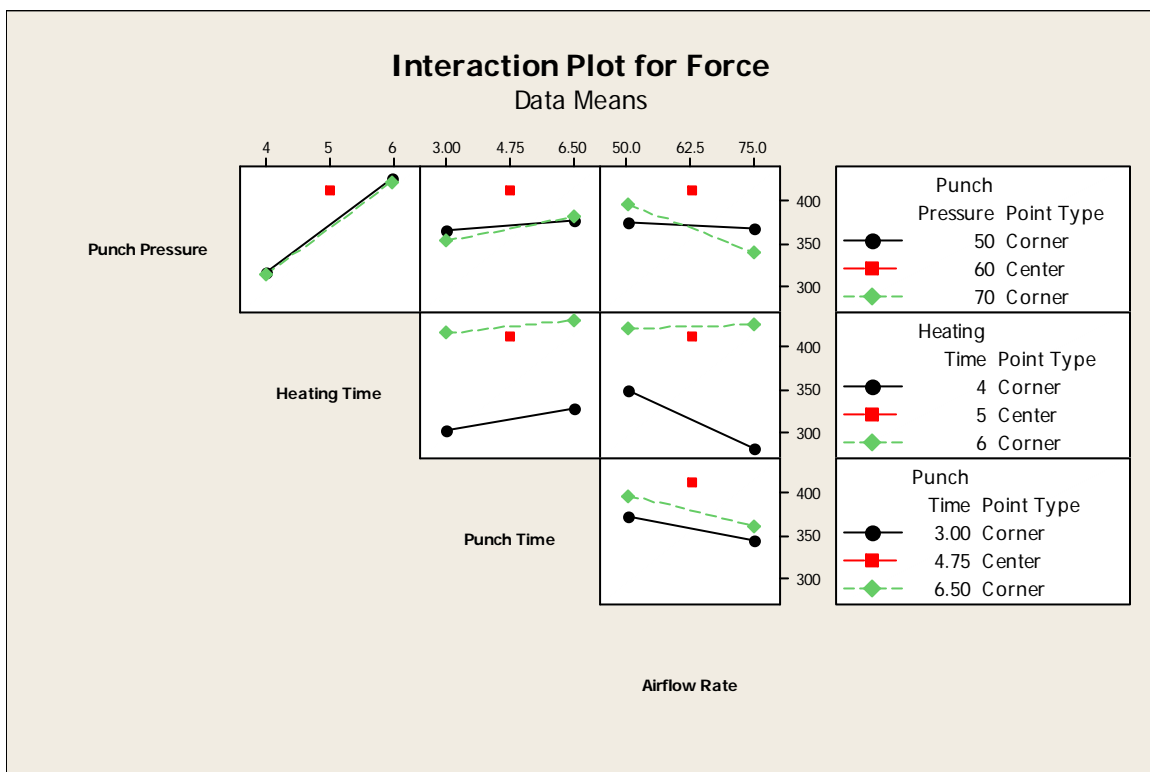


Figure 3-4 Interaction plot for heat stake joint strength analysis

The summary of the Design of Experiment analysis is shown in **Table 3-6** where the significant parameters are highlighted.

Table 3-6 Summary of four-factor-two-level full factorial DOE with center point analysis

Term	Effect	Coef.	SE Coef.	T	P
Constant		368.74	8.067	45.71	0
Punch Pressure	-3.12	-1.56	8.067	-0.19	0.847
Heating Time	110.1	55.05	8.067	6.82	0
Punch Time	20.41	10.21	8.067	1.27	0.209
Airflow Rate	-32.07	-16.04	8.067	-1.99	0.05
Punch Pressure*Heating Time	-1.67	-0.84	8.067	-0.1	0.918
Punch Pressure*Punch Time	8.49	4.25	8.067	0.53	0.6
Punch Pressure*Airflow Rate	-25.56	-12.78	8.067	-1.58	0.117
Heating Time*Punch Time	-5.02	-2.51	8.067	-0.31	0.757
Heating Time*Airflow Rate	36.47	18.24	8.067	2.26	0.026
Punch Time*Airflow Rate	-3.58	-1.79	8.067	-0.22	0.825
Punch Pressure*Heating Time*Punch Time	-9.43	-4.71	8.067	-0.58	0.561
Punch Pressure*Heating Time*Airflow Rate	14.25	7.13	8.067	0.88	0.379
Punch Pressure*Punch Time*Airflow Rate	9.98	4.99	8.067	0.62	0.538
Heating Time*Punch Time*Airflow Rate	18.71	9.36	8.067	1.16	0.249
Punch Pressure*Heating Time*Punch Time*Airflow Rate	5.75	2.88	8.067	0.36	0.722
Centre Point	42.70	33.26			0.203

From **Table 3-6**, the coefficients for the significant terms are selected from the “Coef” column to form the strength response equation Y in Newtons:

$$Y = 55.05*(HT) -16.04*(AR) + 18.24*(HT*AR) + 368.74$$

Where: AR, HT, and HT*AR represent the Airflow Rate, Heating Time, and the interaction effect between Heating Time and Airflow Rate, respectively. The coefficients were calculated such that each term is in coded units with a lower limit value of -1 and a high limit value of +1.

From the full factorial strength analysis, it was confirmed that an interaction effect between Heating Time and Airflow Rate existed. Since there was an interaction effect, the response was not simply the additive function of the four main effects and thus, the L9 analysis could not be applied²⁵. Without the L9 analysis, it was not possible to capture the potential curvilinear relationship of each main effect. However since the center point significance value was 0.203 (greater than a p-level value of 0.05)²⁶, it signifies that a curvature relationship does not exist, and thus the L9 analysis was not required.

3.6 Heat Stake Visual Quality Analysis

The heat stake joint visual quality data for the four-factor-two-level full factorial array from Table 3-3 are entered into the Minitab Design of Experiments. Similar to the joint strength analysis in Section 3.5 the significant effects are found by utilizing the Minitab solver. The Pareto chart in Figure 3-5 shows the significant effects contributing to the visual quality.

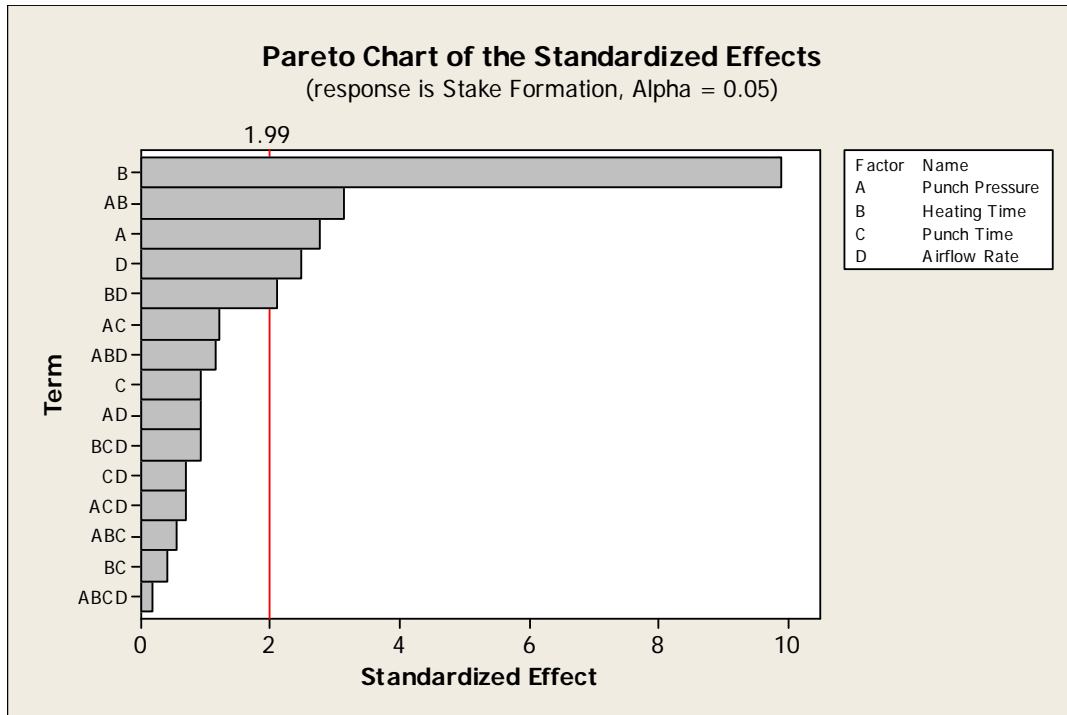


Figure 3-5 Pareto chart for heat stake joint visual quality rating

Using the same alpha risk value of 0.05, the significant factors are:

- Heating Time
- Punch Pressure*Heating Time
- Punch Pressure
- Airflow Rate
- Airflow Rate*Heating Time

The main and interaction effect plots are shown in Figure 3-6 and Figure 3-7 respectively. From the main effect plot, it can be seen that heating time is once again the most significant factor as is deduced from its steeply sloped curve. It has the largest effect on the visual quality compared to all other factors. This is followed by the Punch Pressure, and Airflow Rate factors. Punch time is irrelevant since its main effect plot is almost horizontal.

The interaction effects plot (Figure 3-7) indicates that from the two significant ($\alpha \leq 0.05$) interaction effects (Punch Pressure*Heating Time, and Heating Time*Air Flow Rate) the Punch Pressure*Heating Time interaction contributes more strongly to the visual quality as the lines from its graph display an increased perpendicular interaction compared to the Heating Time*Air Flow Rate interaction.

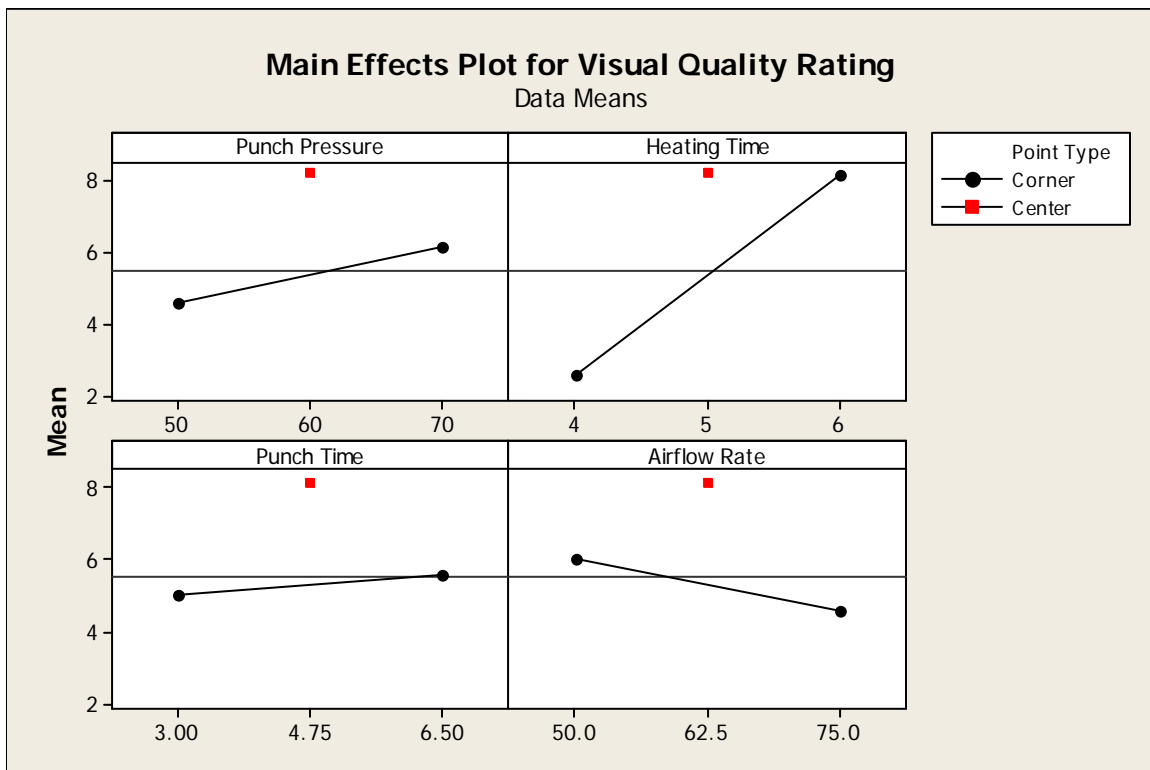


Figure 3-6 Main effects plot for heat stake joint visual quality rating

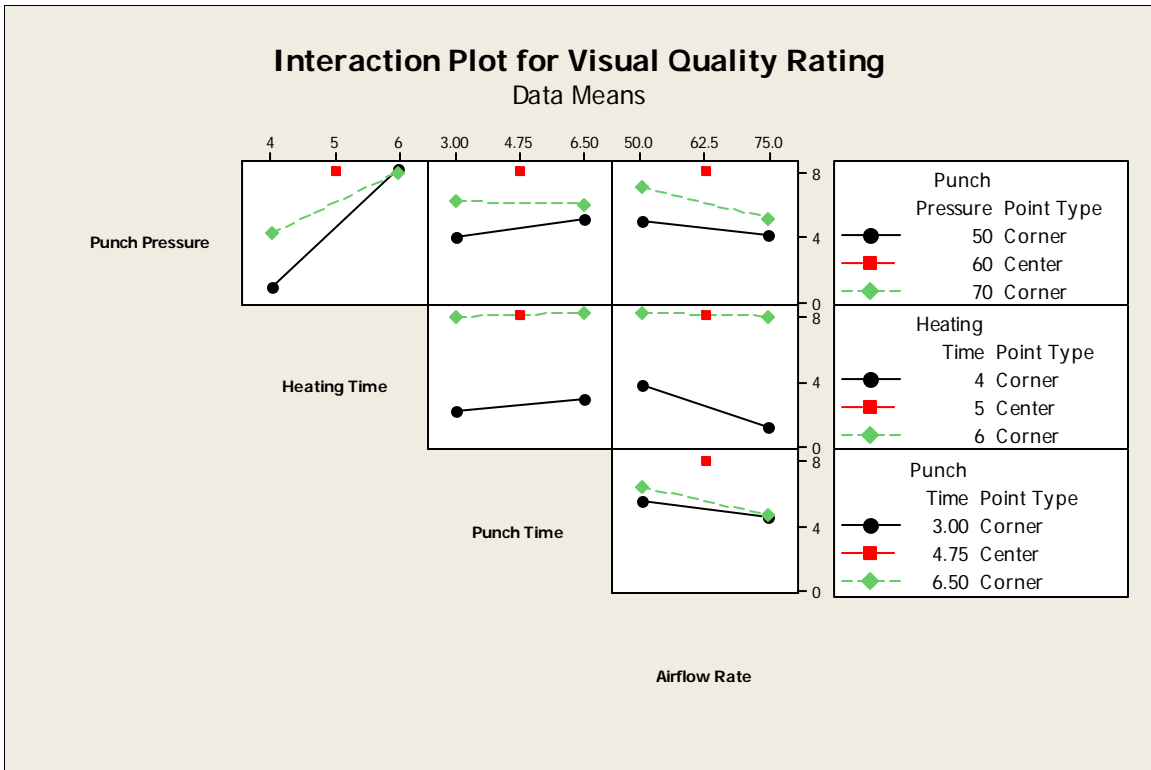


Figure 3-7 Interaction plot for heat stake visual quality rating

The summary of the Design of Experiment analysis is shown in Table 3-7 where the significant effects are highlighted.

Table 3-7 Heat stake joint visual rating analysis summary

Term	Effect	Coef	SE Coef	T	P
Constant		5.3438	0.2831	18.88	0
Punch Pressure	1.5625	0.7813	0.2831	2.76	0.007
Heating Time	5.6042	2.8021	0.2831	9.9	0
Punch Time	0.5208	0.2604	0.2831	0.92	0.36
Airflow Rate	-1.3958	-0.6979	0.2831	-2.47	0.016
Punch Pressure*Heating Time	-1.7708	-0.8854	0.2831	-3.13	0.002
Punch Pressure*Punch Time	-0.6875	-0.3437	0.2831	-1.21	0.228
Punch Pressure*Airflow Rate	-0.5208	-0.2604	0.2831	-0.92	0.36
Heating Time*Punch Time	-0.2292	-0.1146	0.2831	-0.4	0.687
Heating Time*Airflow Rate	1.1875	0.5938	0.2831	2.1	0.039
Punch Time*Airflow Rate	-0.3958	-0.1979	0.2831	-0.7	0.486
Punch Pressure*Heating Time*Punch Time	0.3125	0.1563	0.2831	0.55	0.582
Punch Pressure*Heating Time*Airflow Rate	0.6458	0.3229	0.2831	1.14	0.257
Punch Pressure*Punch Time*Airflow Rate	0.3958	0.1979	0.2831	0.7	0.486
Heating Time*Punch Time*Airflow Rate	0.5208	0.2604	0.2831	0.92	0.36
Punch Pressure*Heating Time*Punch Time*Airflow Rate	-0.1042	-0.0521	0.2831	-0.18	0.854

Once again, taking the coefficients listed in the “Coef” column of Table 3-7, the Visual Quality response equation V can be modelled as:

$$V = 0.07813(PP)+2.8021(HT)-0.6979(AR)-0.8854(PP*HT)+0.5938(HT*AR)+ 5.3438$$

Where HT, PP, AR, PP*HT and HT*AR represent the Heating Time, Punch Pressure, Airflow Rate and the interaction effect between Punch Pressure*Heating Time, and Heating Time*Airflow Rate respectively. The coefficients are once again calculated for the terms in coded units with a lower limit value of -1 and a high limit value of +1.

3.7 Optimization

With both the strength and visual quality response equations derived, optimization was performed to derive a setting of parameters which maximizes both responses. The “Solver” tool in Microsoft Excel was used to perform the optimization.

3.7.1 Optimizing Joint Strength

The joint strength response was the target value which needed to be maximized. Lower and upper boundary constraints of -1 and +1 respectively were placed on Heating Time and Air Flow Rate. Table 3-8 shows the optimal settings of Heating Time and Air Flow Rate at which strength is maximized.

Table 3-8 Control factor setting for optimal strength response

Factor	Settings (Coded Units)	Settings (Uncoded Units)
Heating Time	1	6 s
Airflow Rate	1	70 cfm
Strength Response		425.99N

3.7.2 Optimizing Visual Quality

The visual quality rating response was the target value which needed to be maximized. Lower and upper boundary constraints of -1 and +1 respectively were placed on Heating Time, Punch Pressure, and Airflow Rate. Table 3-9 lists the optimal settings of Heating Time, Punch Pressure, and Airflow Rate at which visual quality is maximized.

Table 3-9 Control factor setting for optimal visual quality response

Factor	Settings (Coded Units)	Settings (Uncoded Units)
Punch Pressure	1	70 psi
Heating Time	1	6 s
Airflow Rate	-1	50 SCFH
Visual Quality Response		8.1459

3.8 Final Optimization of Heat Staking Process Parameters

Since a longer heating time was a common significant factor to both higher strength and visual quality, there must exist a correlation between high visual quality and high joint strength. However, high visual quality is not the causation of high joint strength. This absence of causation is the result of the existence of the Punch Pressure which is observed to affect visual quality but not the joint strength. Nevertheless, high visual quality, which is defined as flash presence on the full circumference of the heat stake head does indeed correlate to a high heat stake joint strength. This result supports the notion that a high heating time will allow the heat staking equipment to plasticize the material more completely, which is essential to create a complete dome surrounded by flash.

From Table 3-8 and Table 3-9, it was observed that the Heating Time and Airflow Rate parameters were relevant factors for both the joint strength and visual quality responses. However, a high Airflow rate is required to maximize strength, and a low setting is required to maximize visual quality. Herein lies the issue of selecting one set of machine parameters to optimize both factors. Table 3-10 below indicates a final set of

machine parameters that are recommended to achieve the strongest joints, as well as consistently high visual quality ratings.

Table 3-10 Process parameter setting values after optimization

Factor	Settings (Coded Units)	Settings (Uncoded Units)
Punch Pressure	1	70 psi
Heating Time	1	6 s
Airflow Rate	1	70 SCFH
Punch Time	1	6.5 s
Strength Response		425.99N
Visual Quality Rating		7.9377

There is a trade-off between setting the airflow rate on at 70 SCFH (high) and 50 SCFH (low), where a high setting will increase the strength while a low setting will increase the visual quality rating. While both the strength and visual quality equations reflect that the factor punch time does not significantly affect either value, it is believed that a longer punch time allows the heat stake more time to cool and maintain a better form, thus punch time has been selected as 6.5 seconds (high).

3.8.1 Validating Optimal Strength Values

The proposed optimal settings are identical to the parameter settings in experiment sixteen (Table 2-2). The average measured strength response of experiment sixteen (Table 3-1) was 440.6 N. To validate the predicted optimal strength response in Table 3-10, it must be compared as a percentage error to the sample population mean (μ) of experiment sixteen.

$$\%Error = \frac{\mu_{sample16} - \mu_{prediction}}{\mu_{sample16}} = \frac{486.6 - 425.99}{486.6} = 3.3\%$$

The predicted strength response is within 3.3% of the sample mean at the optimal settings. This is an extremely close agreement as validation of the predictive equation only requires 10% agreement between the predicted response and the sample mean of experiment sixteen²⁷.

3.8.2 Validating Optimal Visual Quality Values

A similar procedure is performed to validate the predicted visual quality response at the optimal values, against the average measured visual quality response of experiment sixteen. The average measured visual quality response of experiment sixteen is 8.17 (Table 3-3).

$$\%Error = \frac{\mu_{sample16} - \mu_{prediction}}{\mu_{sample16}} = \frac{8.17 - 7.94}{8.17} = 2.8\%$$

The predicted strength response is within 2.8% of the sample mean at the optimal settings. This percentage error is an extremely close agreement as validation of the predictive equation only requires 10% agreement between the predicted response and the sample mean of experiment sixteen²⁸.

3.9 Potential Failure Modes of the Heat Staking Process

Running the heat staking machine at settings other than the optimal settings listed in Table 3-10 resulted in several instances of visual, and strength quality criteria failures. The failure modes were all related to the set of visual and strength quality criteria listed in Table 1-1. Table 3-11 below lists the typical failure modes associated with setting select machine parameters at non-optimal values.

Table 3-11 Potential failure modes associated with non-ideal settings

Machine Parameter Settings	Potential Failure Mode
Short Heating Time (less than 5 seconds) Low Punch Pressure (less than 60 psi)	<ul style="list-style-type: none"> • Incomplete formation of head <ul style="list-style-type: none"> ○ Irregular dome shape • Head not fully seated • Failure of machine to perform punch operation – machine enters error state • Poor Strength – less than 267 N

Shorter heating time results in insufficient heating of the heat stake post. Without reaching the required semi-molten state, the post resists being deformed into the correct dome shaped head. This resistance becomes a more serious issue if the Punch Pressure is low, as the punch head is unable to compress the material. This resistance to flow contributes to restricting the base of the head from fully seating itself onto the surface of the circuit board. If the post is severely under heated, and the punch pressure is set lower than the ideal setting, the machine is unable to press onto the head, and will enter into an error state.

4 Conclusion and Recommendations

The overall goal of the project was to characterize the heat staking process, and establish optimal settings for maximizing the quality of the heat stake joint. This goal was achieved through the derivation of the predictive strength and visual quality response equations.

A guideline for the machine parameter settings was developed through optimization of the predictive equations. Prior to running the optimized settings, the process achieved an average tensile joint strength of 320 N. The optimal joint strength was predicted to be 426 N, and experimentally found to average at 440 N. This shows good agreement between the prediction and empirical result with a percentage error of only 3.3 percent. Changing from the nominal to the predicted optimal settings, the heat stake joint strength increased by 106 N (thirty-three percent increase).

Another aspect of characterizing the heat staking process involved discovering the correlation between visual quality (flash coverage) and the strength of the joint. Seventy-nine percent of flash coverage was predicted as the optimum value to which the strongest joints correlate. This average amount of coverage was verified to be correct within 2.8 percent compared to the flash coverage of the strongest joint experimentally tested. The recommendation that stems from this result is that Autoliv should use the machine settings listed in Table 3-10, and ensure each heat stake joint is produced with at least seventy-five percent flash coverage.

The relationships between the process parameters and the quality of the heat stake joint were developed from the implementation and analysis of the four-factor-two-level full factorial design of experiment. Initially there was no confirmation of the relevant versus irrelevant process parameters and thus the experiments included Punch Time as a control factor. However after performing the analysis, Punch Time was discovered to be irrelevant to the quality of the heat stake joint. Screening experiments in the initial stages of the project would have indicated the irrelevance of Punch Time as a control factor. Having this knowledge early would have enabled the use of a three-factor-two-level full factorial design of experiment, and effectively reduced the required number of experiments by a minimum of eight trials.

This project has a considerable impact on Autoliv's use of the heat staking process. The discovered correlation between well surrounded flash and high joint strength allows Autoliv to implement a simple visual inspection criterion to pass modules. Currently Autoliv is in the process of installing and calibrating an automated visual inspection station within the heat stake assembly line. This system will utilize the recommended seventy-five percent minimum flash coverage as the pass criterion.

The analysis of the effects of the process parameters was based on a constant heat stake post input with fixed geometric properties. Future studies can be conducted with broader scopes to understand the effects of post geometry variations on the quality of the heat stake joint. Variations were also observed between heat stake nozzles. Custom

setting calibration tests can be conducted in the future for each nozzle to produce a more consistent quality of heat stake joints.

From this project, Autoliv gained a better understanding of the dominant process parameters driving the heat staking process. The optimal setting of machine parameters recommended earlier, together with this understanding enables Autoliv to tailor their process to produce optimal quality joints. This knowledge can be applied to their current and future generation of products.

5 References

¹ "Plastic Joining - Staking." TWI.

<http://www.twi.co.uk/content/main_home_index.html>. 2001

² Autoliv Inc. Corporate Engineering Specification GM SDM10/11. Tech. no. CES E323776. 2008 (26)

³ Ruparelia, Samir. "Heat Stake Project Review Meeting." Personal interview. 10 Oct. 2008.

⁴ Nacson, David. Product Design. Toronto: Utpprint, 2009 (Section 6 Page 13).

⁵ "Introduction to Taguchi Method." 26 Aug. 2000.

<http://www.ee.iitb.ac.in/~apte/cv_pra_taguchi_intro.htm>.

⁶ Ibid

⁷ Nacson (Section 6 Page 18)

⁸ Nacson (Section 6 Page 19)

⁹ Nacson (Section 6 Page 31)

¹⁰ Nacson (Section 6 Page 15)

¹¹ Nacson (Section 6 Page 16)

¹² Nacson (Section 6 Page 31)

¹³ Mason, Robert L., Richard F. Gunst, and James L. Hess. Statistical Design and Analysis of Experiments: With Applications to Engineering and Science. 2nd ed. Wiley-IEEE, 2003 (253).

¹⁴ Mason (254)

¹⁵ Nacson (Section 8 Page 16)

¹⁶ Ibid

¹⁷ Nacson (Section 6 Page 31)

¹⁸ Ruparelia, Samir. "Heat Stake Project Review Meeting." Personal interview. 28 Nov. 2008.

¹⁹ Autoliv Inc. Corporate Engineering Specification GM SDM10/11. Tech. no. CES E323776. 2008 (25)

²⁰ Nacson, David. "Estimates for Consulting Charges Relating to Design of Experiments." E-mail to Royston De Souza. 14 Mar. 2009.

²¹ Ibid

²² Nacson (Section 6 Page 31)

²³ Easton, Valerie J., and John H. McColl. "Statistics Glossary - hypothesis testing." University of Glasgow: Statistics. 24 Mar. 2009
<http://www.stats.gla.ac.uk/steps/glossary/hypothesis_testing.html>.

²⁴ Ibid

²⁵ Mason (254)

²⁶ Easton, Valerie J., and John H. McColl. "Statistics Glossary - hypothesis testing." University of Glasgow: Statistics. 24 Mar. 2009
<http://www.stats.gla.ac.uk/steps/glossary/hypothesis_testing.html>.

²⁷ Nacson (Section 7 Page 31)

²⁸ Ibid